

---

## A pollen-climate calibration from western Patagonia for palaeoclimatic reconstructions

Montade Vincent <sup>1,\*</sup>, Peyron Odile <sup>2</sup>, Favier Charly <sup>2</sup>, Francois Jean Pierre <sup>3</sup>, Haberle Simon G. <sup>4,5</sup>

<sup>1</sup> Georg August Univ Gottingen, Albrecht von Haller Inst Plant Sci, Dept Palynol & Climate Dynam, Gottingen, Germany.

<sup>2</sup> Univ Montpellier, ISEM, CNRS, EPHE,IRD, Montpellier, France.

<sup>3</sup> Univ Playa Ancha, Fac Ciencias Nat & Exactas, Dept Ciencias Geog, Valparaiso, Chile.

<sup>4</sup> Australian Natl Univ, Dept Archaeol & Nat Hist, Sch Culture Hist & Language, Coll Asia & Pacific, Canberra, ACT, Australia.

<sup>5</sup> Australian Natl Univ, ARC Ctr Excellence Australian Biodivers & Heritag, Canberra, ACT, Australia.

\* Corresponding author : Vincent Montade, email address : [vincent.montade@gmail.com](mailto:vincent.montade@gmail.com)

---

### Abstract :

Palaeoecological studies of sediment records from the western margins of southern South America have revealed vegetation dynamics to be under the influence of major regional climate drivers such as the Southern Westerly Winds, Southern Annular Mode and El Nino Southern Oscillation. Despite the substantial number of palynological records in this region, very few quantitative pollen-based climate reconstructions using surface samples have been made. In this context, our objective was first to investigate the modern pollen-vegetation-climate relationships in the western Patagonian. The results show that the modern pollen dataset reflects the main vegetation types and that summer precipitation and winter temperature represent the main climate parameters controlling vegetation distribution. Secondly using this pollen-climate dataset we evaluate and compare the performance of two models (Weighted Averaging Partial Least Squares and Modern Analog Technique). We used these models to make climate reconstructions from two oceanic pollen records from western Patagonia. Compared with independent climate indicators, our pollen-inferred climate reconstructions reveal the same overall trends, showing the potential of pollen-climate transfer functions applied to this region. This study provides much needed data for quantitative climate reconstructions in South America, but which also needs to be improved by enlarging the modern pollen dataset.

**Keywords** : palaeoclimate, pollen, quantitative climate reconstruction, South America, western Patagonia

## 45 **1. Introduction**

46 The latitudinal distribution of the main plant communities in western Patagonia closely  
47 follows the climate gradient across the region (Schmithüsen, 1956; Gajardo, 1994). In  
48 addition to temperatures decreasing southward, rainfall shows a strong increase southward  
49 directly related to the intensity of the Southern Westerly Wind (SWW) belt (Garreaud *et al.*,  
50 2013). In particular, models and palaeoclimate archives reveal the importance of the SWW  
51 belt through their role in regional climate change, **alongside the growing recognition of the**  
52 **role of the Southern Annular Mode and El Niño Southern Oscillation phenomenon in**  
53 **modulating regional climate through time (e.g. Toggweiler *et al.*, 2006; Anderson *et al.*, 2009;**  
54 **Moreno *et al.*, 2014).** A substantial number of records based on palynological studies have  
55 thus been produced in this region with a focus on questions regarding the behaviour of the  
56 SWW belt at different timescales (see Flantua *et al.*, 2015 and literature therein). Western  
57 Patagonia is one of the regions from South America with the most pollen records and these  
58 studies have sometimes led to different conclusions regarding the long-term dynamics of the  
59 SWW belt (e.g. Kilian and Lamy, 2012). To explain those discrepancies new records are  
60 required in regions where the density of palaeoecological data is lower, such as in the Chilean  
61 channel region (47° to 53°S). On the other hand, to explain those discrepancies, it also  
62 requires improvement of the methods to reconstruct the climate. Indeed, most palaeodata from  
63 this region are based on qualitative climate reconstructions, which may limit the interpretation  
64 of multi-site comparisons for reconstructing climate variability at a regional scale.  
65 Quantitative climate approaches are thus needed to provide a better understanding of the  
66 regional pattern of climate changes. Such approaches are also essential to perform data-model  
67 comparisons improving our understanding of climate mechanisms and future climate changes  
68 (Harrison *et al.*, 2016). In Patagonia, local modern pollen datasets have been published during  
69 the last two decades to study relationships between pollen, vegetation and sometimes climate

70 (Haberle and Bennett, 2001; Paez *et al.*, 2001; Markgraf *et al.*, 2002; Tonello *et al.*, 2008,  
71 2009; Mancini *et al.*, 2012; Schäbitz *et al.*, 2013). Only three local quantitative climate  
72 reconstructions inferred from fossil pollen records have been provided using some of these  
73 datasets (Markgraf *et al.*, 2002; Tonello *et al.*, 2009; Schäbitz *et al.*, 2013). Hence, further  
74 local studies calibrating the existing modern pollen data to perform quantitative  
75 reconstructions are necessary as a first step to large-scale regional climate reconstructions.  
76 In this context our aim here is to compile modern pollen data from western Patagonia to  
77 investigate the modern pollen-vegetation-climate relationships and to develop climate transfer  
78 functions. We first assemble modern pollen samples to span the range of environmental  
79 values likely to be represented by the main different vegetation types from this region.  
80 Secondly, this paper aims to provide reliable quantitative estimates for seasonal climatic  
81 variables. Multiple methods for pollen-based climate reconstruction including most standard  
82 methods, the Weighted Averaging Partial Least Squares (WA-PLS) and the Modern Analog  
83 Technique (MAT) will be applied and compared. We finally use these models to perform  
84 quantitative climate reconstructions for the last deglaciation and the Holocene inferred from  
85 two pollen records: the core MD07-3104 in the Reloncaví Fjord at 41°S and the core MD07-  
86 3088 offshore Taitao Peninsula at 46°S (Montade *et al.*, 2012, 2013).

87

## 88 **2. Environmental settings**

89 Western Patagonia represents the southern part of South America in Southern Chile extending  
90 from 41° to 56°S (Fig. 1). The Andean Cordillera spreads from north to south with peaks  
91 rarely exceeding 3000 m asl. Along the coast, a secondary mountain range, the Coastal  
92 Range, is rapidly submerged south of 42°S which results in a complex system of fjords,  
93 channels and archipelagos. The combination of these mountain ranges with high-velocity  
94 SWW generates high orographic rainfall increasing southward with SWW intensity increase

95 (Garreaud *et al.*, 2013). During the austral winter the SWW belt spreads northward to 30°S  
96 but remains south of 46-47°S during the austral summer. In the northern part, precipitation  
97 primarily from winter rains, reaches around 2000 mm.yr<sup>-1</sup>. Southwards, seasonality of  
98 precipitation decreases and disappears south of 46°S, where precipitation reaches values over  
99 3000 mm.yr<sup>-1</sup>. East of the Andes, the annual amount of precipitation decreases rapidly to  
100 below 1000 mm. The temperatures contrast with precipitation showing a weak annual  
101 seasonal variability with values remaining above freezing along the coast. However, with the  
102 altitude increase, temperature seasonality increases through the Andes. The climate is thus  
103 considered as temperate to cool-temperate and humid to hyper-humid from north to south at  
104 low elevation. East of the Andes, climate is generally dry and temperate to cool-temperate  
105 from north to south (Garreaud *et al.*, 2009).

106 Vegetation communities in western Patagonia are considered to be strongly influenced by the  
107 gradient of increasing annual precipitation and decreasing annual temperature southward  
108 (Schmithüsen, 1956; Gajardo, 1994; Markgraf *et al.*, 2002; Luebert and Plissock, 2004) (Fig.  
109 1): (i) the Lowland Deciduous Forest, dominated by deciduous trees (i.e. *Nothofagus obliqua*,  
110 *N. alpina*), conifers (i.e. *Saxegothaea conspicua*, *Podocarpus salignus*) and several broadleaf  
111 evergreen elements (i.e. *Aetoxicon punctatum*, *Persea lingue*); (ii) the Valdivian Rainforest,  
112 the most diversified Patagonian forest type, characterized by the codominance of evergreen  
113 trees (i.e. *Nothofagus dombeyi*) with a number of broadleaf evergreen elements (i.e.  
114 *Eucryphia cordifolia*, *Aetoxicon punctatum*, *Caldcluvia paniculata*, and several species of  
115 Myrtaceae); (iii) the North Patagonian Rainforest, dominated by several species of conifers  
116 (i.e. *Fitzroya cupressoides*, *Pilgerodendron uviferum*, *Podocarpus nubigenus*) with some  
117 *Nothofagus* and broadleaf species (i.e. *Nothofagus dombeyi*, *N. nitida*, *N. betuloides*,  
118 *Weinmannia trichosperma*); (iv) the Subantarctic Rainforest, characterized by the  
119 codominance of conifer and *Nothofagus* species (i.e. *Pilgerodendron uviferum*, *Nothofagus*

120 *nitida* and *N. betuloides*); (v) also frequently associated with the Subantarctic Rainforest, the  
121 Magellanic Moorland represented by an open plant community occurring under high  
122 precipitation is characterized by the predominance of peat-bog plants (i.e. *Sphagnum*  
123 *magellanicum*), cushion-bog species (*Astelia pumila*, *Donatia fascicularis*) with graminoid  
124 taxa mainly represented by Cyperaceae or Juncaceae and shrubs (Ericaceae); (vi) the  
125 Subantarctic Deciduous Forest, mainly represented by deciduous trees (i.e. *Nothofagus*  
126 *pumilio* and *N. antarctica*) adapted to cold conditions is also associated with an increase  
127 proportion of graminoids (grasses or sedges) characteristic of to the Andean high elevation  
128 grassland which dominates the landscape above the treeline.

129 Along the altitudinal gradient in northern Patagonia, with increasing orographic precipitation  
130 and decreasing temperatures, a similar sequence of vegetation distribution is observed except  
131 for the Magellanic Moorland which cannot develop under sub-zero temperature values.  
132 Finally, east of the Andes under dry conditions the Patagonian Steppe develops in the  
133 lowlands. The Patagonian Steppe is dominated by herbs and shrubs mainly characterized by  
134 Poaceae, Asteraceae, Cyperaceae, Solanaceae, Apiaceae and Chenopodiaceae.

135

### 136 **3. Material and methods**

#### 137 **3.1. Modern pollen and climate datasets**

138 The modern pollen dataset was compiled using 24 oceanic surface sediments (Montade *et al.*,  
139 2011) and 186 terrestrial surface samples including 139 soils and 47 lakes (Haberle and  
140 Bennett, 2001; Markgraf *et al.*, 2002; Francois, 2014). Much of these surface samples belong  
141 to the northern half of Patagonia, distributed inland on both sides of the Andes (Fig. 1 and  
142 Table S1). Only two samples are located between 47° and 52°S corresponding to oceanic  
143 surface samples in the fjords. Further south, 19 samples are from islands within the fjords and  
144 off-shore near Punta Arenas. After dataset compilation, a total of 78 pollen taxa was obtained

145 (Table S2) by updating the pollen taxa nomenclature followed the harmonization from  
146 Markgraf *et al.* (2002). To this initial harmonization, we added five pollen taxa related to  
147 samples located more southward (*Astelia*, *Caltha*, *Donatia*, *Lepidoceras*, *Luzuriaga*) and  
148 Asteraceae (except *Artemisia*) were merged in two groups: A. *Asteroideae* and A.  
149 *Cichorioideae*. For most of these samples, the pollen sums reach values above 200. Only 11  
150 samples have a sum between 100 and 200; however as the number of surface samples is  
151 relatively limited, we decided to keep these samples in the dataset. Pollen percentages were  
152 calculated on the basis of their respective pollen sums excluding *Rumex* and Polygonaceae as  
153 these taxa are generally related to human impact (Heusser, 2003; Schäbitz *et al.*, 2013).  
154 Although characteristic of aquatic and wetland taxa some Cyperaceae species (sedges) are  
155 also naturally abundant in the Magellanic Moorland or in high elevation grasslands (Markgraf  
156 *et al.*, 2002; Villa-Martínez *et al.*, 2012). For that reason Cyperaceae was kept in the  
157 calculation of the pollen sums. To remove noise for statistical analyses, the data matrix was  
158 reduced to 38 taxa characterized by values above 2% in more than two samples. Furthermore,  
159 in order to provide a better understanding of the relationships between pollen assemblages,  
160 vegetation and climatic parameters from western Patagonia, statistical analyses were  
161 performed on a modern pollen dataset of 183 samples, excluding 27 samples from the initial  
162 dataset (Table S1). We first excluded samples dominated by herbs or shrubs pollen taxa  
163 located east of 71°W in northern half of Patagonia (north of 46°S) that mainly corresponds to  
164 Patagonian steppe controlled by the east-west climate Andean gradient. West of 71°W in  
165 northern half of Patagonia, we also excluded samples dominated by herbs or shrubs which  
166 correspond to samples influenced by human impact reflecting an open landscape vegetation at  
167 low elevation sites (< 500 m asl). We then excluded samples associated with pollen taxa of  
168 Magellanic Moorland from the same area, because their occurrences too far in the north  
169 reflect local edaphic conditions.

170 An unconstrained cluster analysis based on chord distance was performed on the 183 samples  
171 to reveal similarities among pollen assemblages and to provide the order of surface samples  
172 plotted in the pollen diagram (Fig. 2). The different pollen zones identified by the cluster  
173 dendrogram have been ascribed to groups according to pollen assemblages and vegetation  
174 types (Figs. 2 and 3). Climate data calculated at each surface sample location were extracted  
175 from the WorldClim database (Hijmans *et al.*, 2005). The present-day climate parameters  
176 correspond to the annual precipitation sum ( $P_{ANN}$ ) and the precipitation sums during  
177 December-January-February ( $P_{SUM}$ ) and June-July-August ( $P_{WIN}$ ). Temperature values  
178 correspond to the mean values of the same months ( $T_{ANN}$ ,  $T_{SUM}$  and  $T_{WIN}$ ). For each oceanic  
179 sample, the closest on-shore climate values were calculated. In the Andes, because of the  
180 limited spatial resolution, elevational climate values based on WorldClim differ sometimes  
181 from the measured values by several hundred meters. As interpolated temperature values are  
182 very sensitive to the altitudinal gradient, we corrected temperature values using a lapse rate  
183 value of 0.6°C per 100 m. Altitude discrepancies were found to be too small to have a  
184 significant influence on precipitation estimates and no corrections have been done.

185 Based on the same modern pollen dataset, we carried out a Principal Component Analysis  
186 (PCA) on square-root transformed pollen relative frequencies and projected climate variables  
187 on it to determine if, and how, variation in pollen rain is related to climate patterns in western  
188 Patagonia. Square-root transformation of relative frequencies is commonly used as it allows  
189 variance stabilization and ‘signal to noise’ ratio maximization in the data (Prentice, 1980),  
190 which is equivalent to an ordination of pollen spectra using the square chord distance.

191

### 192 **3.2. Quantitative climate reconstruction**

193 The quantitative climate reconstruction is based on a multiple method approach to test the  
194 reliability of the methods for these complex environments and to provide an improved

195 assessment of the uncertainties involved in palaeoclimate reconstructions. Using the R  
196 package RIOJA (Juggins, 2015), we used the MAT based on a comparison of past  
197 assemblages to modern pollen assemblages, and the WA-PLS which requires statistical  
198 calibration. These methods are frequently used in climate reconstruction with their own set of  
199 advantages and limitations; they were successfully used for the Holocene climate  
200 reconstructions from terrestrial and marine records (e.g. Peyron *et al.*, 2011; Mauri *et al.*,  
201 2015; Ortega-Rosas *et al.*, 2016). The MAT (Guiot, 1990) uses the squared-chord distance to  
202 determine the degree of similarity between samples with known climate parameters (modern  
203 pollen samples) to samples for which climate parameters are to be estimated (fossil pollen  
204 sample). The chord distance indicates the degree of dissimilarity between two pollen samples  
205 (small distance = close analogues selected for the climate reconstruction). A minimum  
206 distance corresponding to a minimum 'analogue' threshold is established. Subsequently, each  
207 climate parameter is calculated for each fossil pollen assemblage as the weighted mean of the  
208 climate of the closest modern analogues. The WA-PLS method (ter Braak and Juggins, 1993)  
209 is a transfer function which assumes that the relationship between pollen percentages and  
210 climate is unimodal. The modern pollen dataset used is considered a large matrix with  $n$   
211 dimensions, corresponding to each of the pollen taxa within the dataset. WA-PLS operates by  
212 compressing the overall data structure into latent variables. Several taxa are directly related to  
213 climate parameters of interest. To avoid the co-linearity among the taxa, we can reduce the  
214 matrix into a smaller number of components based on both linear predictors of the parameter  
215 of interest and the residual structure of the data when those predictors are removed. The  
216 modification of PLS proposed by ter Braak and Juggins (1993) requires transformation of the  
217 initial dataset using weighted averaging along a gradient defined by the climate parameter of  
218 interest, such that the pollen taxa that best define the climate gradient are weighted more  
219 heavily than those that show little specificity to the gradient. Ter Braak and Juggins (1993)



220 detail the importance of using cross validation to assess and select WA-PLS models and show  
221 that statistics based on cross-validation provide more reliable measures of the true predictive  
222 ability of the transfer functions.

223 We then evaluate the performance of models using a leave-one-out cross-validation test  
224 performed with the training set of 183 modern pollen samples (38 pollen taxa). We also test  
225 the reliability of the transfer functions applied to oceanic pollen assemblages by  
226 reconstructing the climate conditions from 24 oceanic surface sediment samples (these  
227 oceanic samples were previously removed from the 183 modern pollen-climate training set  
228 before to do this test). We further check the extent to which calibration may be affected by  
229 spatial autocorrelation using the R package PALAEOSIG (Telford, 2015). Finally we apply  
230 the models to two oceanic pollen records: the core MD07-3104 located at 41°S in the  
231 Reloncaví Fjord and the core MD07-3088 located at 46°S offshore Taitao Peninsula (Montade  
232 *et al.*, 2012, 2013).

233

## 234 **4. Results and discussion**

### 235 **4.1. Vegetation–pollen-climate relationships**

236 The pollen spectra were divided into eleven zones according to the cluster analysis (Fig. 2).  
237 Because of limitations of morphological pollen identifications, most of the pollen taxa include  
238 several species, which explains the high proportion of some taxa in different pollen zones. In  
239 particular, the most abundant one, *Nothofagus dombeyi*-type includes five tree species (*N.*  
240 *dombeyi*, *N. pumilio*, *N. antarctica*, *N. betuloides*, *N. nitida*) growing in the different  
241 Patagonian environments. Based on the fluctuations of this pollen type associated and the  
242 dominant pollen taxa, we combined the pollen zones in six groups to reflect the main  
243 vegetation types and their ecological affinity (Figs. 2 and 3). In the grassland group which  
244 corresponds to three pollen zones, *Nothofagus dombeyi*-type remains below 20%. Samples are

245 generally dominated by at least one herbaceous taxon, reaching more than 25% (Poaceae,  
246 Cyperaceae, Asteraceae *Asteroideae* or Apiaceae). Most of samples of this group occur in the  
247 northern half of Patagonia in the Andes and correspond to an open landscape vegetation  
248 characterized by high elevation grassland partly influenced by the Subantarctic Deciduous  
249 Forest. Southward, samples that also corresponding to an open landscape vegetation are  
250 associated with the Magellanic Moorland. Although characterized by different species, low  
251 resolution pollen identification for non-arboreal taxa (mainly family) makes it difficult to  
252 differentiate open vegetation between high elevation and lowland environments (Markgraf *et*  
253 *al.*, 2002). Included in the same group, these samples from different environments reflect the  
254 importance of precipitation variability (Fig. 3b) and winter temperatures, that are decreasing  
255 with altitude or southward attaining low values in winter ( $\sim 3^{\circ}\text{C}$ ). The Subantarctic Deciduous  
256 Forest (SDF) group includes two pollen zones (Fig. 2), either dominated by *N. dombeyi*-type  
257 ( $> 60\%$ ) or co-dominated by *N. dombeyi*-type ( $> 50\%$ ) and Cyperaceae (15-35%). These  
258 assemblages are mainly distributed across the Andean relief in the northern half of Patagonia  
259 with precipitation slightly higher and temperatures slightly lower than for the grassland group.  
260 Samples co-dominated by Cyperaceae generally occurred above 900 m asl showing the  
261 influence of high elevation grassland. Several samples are also located in the southern part  
262 and five of them are from the islands within the fjords west of the Andes with high yearly  
263 precipitation (Fig. 3). With two pollen zones, the Valdivian Rainforest (VR) group is  
264 characterized by *N. dombeyi*-type remaining generally lower than 30%, accompanied by  
265 significant amounts of arboreal taxa such as Myrtaceae, *Saxegothaea*, *Podocarpus*,  
266 *Weinmannia* or *Gevuina/Lomatia*. Among herbaceous taxa only Poaceae reach values higher  
267 than 10% in this group which could be partly induced by human impact in northwestern  
268 Patagonia. Precipitation ( $2150 \text{ mm}\cdot\text{yr}^{-1}$ ) and annual temperatures ( $10^{\circ}\text{C}$ ) in this region are  
269 higher than in the two previous vegetation groups. The North Patagonian/Valdivian

270 Rainforest (NPR/VR) group (one pollen zone) shows again high amounts of *N. dombeyi*-type  
271 (> 50%), however the tree taxa *Podocarpus*, Cupressaceae, Myrtaceae and *Tepualia* replace  
272 herbaceous taxa in comparison with the SDF group. This group occurs in the northern half of  
273 Patagonia throughout the Andes and along the coast with generally high amounts of  
274 precipitation (2300 mm.yr<sup>-1</sup>) and annual temperatures around 9°C. Only two samples from  
275 this group occur south of this domain probably related to their high frequencies of conifers.  
276 The North Patagonian/Subantarctic Rainforest (NPR/SR) group is represented by two pollen  
277 zones. It differs from NPR/VR group by lower values of *N. dombeyi*-type (< 40%) at the  
278 expense of Cupressaceae (max. up to 93%), *Podocarpus* and *Tepualia*. Samples are located in  
279 the same region than NPR/VR group with similar temperatures and slightly higher  
280 precipitation (2466 mm.yr<sup>-1</sup>). Abundant in the NPR/VR and NPR/SR groups, the arboreal  
281 pollen taxon Cupressaceae includes three conifers, *Fitzroya cupressoides*, *Pilgerodendron*  
282 *uviferum* and *Austrocedrus chilensis*. The last one grows under colder and drier conditions  
283 than *F. cupressoides* and *P. uviferum* which are characteristic of very humid conditions  
284 mainly west of the Andes. Consequently, as discussed by Markgraf *et al.* (2002), the  
285 Cupressaceae pollen taxon may introduce some noise in climatic values of these two groups.  
286 In the Subantarctic Rainforest/Magellanic Moorland (SR/MM) group characterized by one  
287 pollen zone, pollen assemblages are mostly characterized by herbaceous or shrubby taxa with  
288 Ericales, *Myzodendron*, *Astelia*, Juncaceae and *Caltha* with *N. dombeyi*-type fluctuating  
289 between 30 and 50%. The pollen taxon *Astelia* characteristic of *A. pumila* only growing in the  
290 Magellanic Moorland is a very good indicator of this vegetation type. This group only occurs  
291 in southern Patagonia and the low seasonality of precipitation and temperature allows us to  
292 distinguish this vegetation group from the other ones (Fig. 3).

293 Distribution of samples in the PCA diagram (Fig. 4b) along the axis-1 reflects the variation  
294 from the vegetation in an open landscape (grassland and SR/MM groups) mixed with the SDF

295 group to the rainforest groups. Along axis-2, the distribution of samples mainly reflects the  
296 vegetation from the SR/MM, NPR/SR, NPR/VR groups to grassland and VR groups.  
297 Projection of climatic parameters in the PCA shows that the axis-1 is mainly correlated with  
298 temperatures while axis-2 is mainly correlated with precipitation (Fig. 4). In particular, the  
299 highest  $r^2$  for axis-1 and -2 corresponding to  $T_{WIN}$  (0.55) and  $P_{SUM}$  (0.47), respectively,  
300 support the notion that parameters represent the main climatic limiting factors in western  
301 Patagonia determining vegetation distribution. This result is not surprising considering the  
302 vegetation distribution in western Patagonia which is characterized by a southward winter  
303 temperature decrease and a summer precipitation increase reducing rainfall seasonality (Fig.  
304 1). A temperature decrease is also partly observed with altitude increase across the Andes in  
305 the northern half of western Patagonia where the rainforests is replaced by the SDF  
306 sometimes mixed with grasslands. Although we have a spatial gap in the sample distribution  
307 between  $47^\circ$  and  $52^\circ S$ , corresponding to the region where Magellanic Moorland mixed with  
308 the Subantarctic Rainforest is found, we partly capture the regional pattern of vegetation and  
309 climate conditions from this part of Patagonia with the samples located further south along the  
310 coast ( $52-53^\circ S$ ). In particular, under high annual rainfalls and a weak seasonality of  
311 precipitation and temperatures, these samples reflect similar climate and vegetation conditions  
312 with the region located from  $47^\circ$  to  $48^\circ S$ .

313

## 314 **4.2. Model performance**

### 315 **4.2.1. Specificity of oceanic samples in western Patagonia**

316 An important requirement in quantitative paleoenvironmental reconstruction is the need of a  
317 high-quality training set of modern samples. The training set should be (1) representative of  
318 the likely range of variables, (2) of highest possible taxonomy detail, (3) of comparable  
319 quality and (4) from the same sedimentary environment (Brewer *et al.*, 2013). The last point

320 can be particularly discussed because, due to our limited set of modern pollen samples, we  
321 decided to compile samples from different depositional environments (soil, lake and oceanic).  
322 Different depositional environment and taphonomic processes mainly between terrestrial and  
323 oceanic samples could affect significantly our pollen assemblages. Oceanic samples in  
324 particular should reflect a more regional signal than the terrestrial ones. However, it has been  
325 shown that the pollen signal from oceanic samples in this region remains relatively local to  
326 the vegetation from the nearby continental area (Montade *et al.*, 2011). This is mainly  
327 explained by the local transport conditions: under strong westerlies blowing throughout the  
328 year, the aeolian sediment input (including pollen) to the ocean is minimized and the pollen  
329 are mainly brought by strong fluvial discharges coming from short rivers restricting the  
330 sediment provenance. Probably partly related to these specific local conditions, it did not  
331 appear that these different depositional environments substantially affected pollen  
332 assemblages (Montade *et al.*, 2011).

333 To test the reliability of the transfer functions applied to oceanic pollen assemblages, we  
334 applied the WA-PLS and the MAT to the 24 oceanic surface sediment pollen samples,  
335 considered here as “fossil samples” (Fig. S1). The comparison between reconstructed and  
336 observed values for the main climatic limiting factor in western Patagonia,  $P_{SUM}$  and  $T_{WIN}$   
337 shows a higher  $r^2$  for the WA-PLS (0.56 and 0.67) than for the MAT (0.37 and 0.31). These  
338 correlations are explained by a general southward precipitation increase and temperature  
339 decrease, evidenced by both, reconstructed and observed values. However, some differences  
340 are observed. One of the most obvious concerns the reconstructed  $P_{SUM}$  values: while  
341 observed  $P_{SUM}$  reach maxima between 47° and 52°S, where the Subantarctic Rainforest mixed  
342 with the Magellanic Moorland occurs, the reconstructed values are much lower than observed.  
343 This may be explained by a lack of terrestrial samples between 47° and 52°S. In particular,  
344 the oceanic pollen samples at these latitudes are reconstructed with terrestrial samples from

345 Subantarctic Rainforest located to the north and not with the rainforest mixed with the  
346 Magellanic Moorland growing under very wet conditions. Concerning  $T_{WIN}$ , north of 47°S,  
347 reconstructed values are almost all underestimated. A large part of the terrestrial pollen  
348 dataset is located throughout the Andes, while the oceanic pollen dataset is located along the  
349 coast. Consequently temperature seasonality higher in the Andes induces lower reconstructed  
350  $T_{WIN}$  than observed temperature along the coast. Despite these differences, explained by a  
351 lack of modern pollen samples, the MAT and the WA-PLS are able to reconstruct the general  
352 pattern of north-south climate gradient from oceanic pollen samples. Furthermore these  
353 results suggest that the WA-PLS seems more accurate than the MAT to reconstruct the overall  
354 latitudinal climate trends through western Patagonia.

355

#### 356 **4.2.2. Evaluation of the WA-PLS and the MAT models**

357 After the first test on the oceanic pollen samples, we analysed the performance of the MAT  
358 and the WA-PLS transfer functions using the total 183-training set with a leave-one-out cross-  
359 validation. Prior to final model development, we checked for ‘outliers’, i.e. the modern pollen  
360 samples producing extreme values. Two outliers for  $P_{SUM}$  were identified in both, the MAT  
361 and the WA-PLS (Fig. S2). A third outlier was identified with  $P_{SUM}$  reconstructed by the WA-  
362 PLS showing a high negative value (ca. -500 mm). Such a value seems to be associated with a  
363 high percentage of *Araucaria* (>40%) reflecting a local signal from the vegetation. These  
364 three outliers were excluded from the training set. The final transfer functions was then  
365 performed on a 180-training set (Table 1 and Fig. 5). The optimal number of components to  
366 include in the WA-PLS model was assessed by a cross-validation following the procedure of  
367 ter Braak and Juggins (1993). A leave-one-out cross-validation has been selected here. A two  
368 component WA-PLS model was then selected on the basis of the low root mean square error  
369 of prediction (RMSEP), low maximum bias, and high  $r^2$  between observed and predicted

370 values of  $P_{SUM}$  and  $T_{WIN}$  (Table 1). For the MAT, we retain the four nearest analogues for an  
371 optimal reconstruction.

372 The performance of our models is summarized in the Table 1. The RMSEP of the WA-PLS  
373 model is of ca. 164 mm for  $P_{SUM}$  and ca. 1.6°C for  $T_{WIN}$ . The  $r^2$  between the observed climate  
374 values and those predicted by the WA-PLS (MAT) model is 0.53 (0.54) and 0.55 (0.77) for  
375  $P_{SUM}$  and  $T_{WIN}$  respectively. Equivalent for  $P_{SUM}$ , the diagnostic statistics of MAT shows  
376 better scores for  $T_{WIN}$  mainly concerning the  $r^2$ . However, several studies suggest that MAT  
377 may produce over-optimistic diagnostics when cross-validation is limited to leave-one-out  
378 model (Telford and Birks, 2005). Low values of  $T_{WIN}$  are overestimated with both methods,  
379 particularly with the WA-PLS (Fig. 5). We also observed an underestimation of the high  $P_{SUM}$   
380 values, particularly with the MAT.

381 The calibration seems robust and adequately model taxa and their environments with lowest  
382 possible error of prediction and the lowest bias values (Table 1). However, the good  
383 performance of the methods and the high correlations between climatic variables may also be  
384 discussed according to the potential problem of the spatial autocorrelation in transfer  
385 functions pointed out by Telford and Birks (2005). Spatial autocorrelation is the tendency of  
386 sites close to each other to resemble one another more than randomly selected sites. Telford  
387 and Birks (2005) argued that the estimation of the performance and the predictive power of a  
388 training set by cross-validation assume that the test set must be statistically independent of the  
389 training set and that a cross-validation in the presence of spatial-autocorrelation seriously  
390 violate this assumption as the samples are not always spatially and statistically independent.  
391 Therefore, in case of strong autocorrelation, the RMSEP on cross validation is overoptimistic.  
392 The importance of spatial autocorrelation in transfer functions evidenced by Telford and Birks  
393 (2005) has been discussed by several authors (Telford and Birks, 2005; Guiot and de Vernal,  
394 2007; Fréchet *et al.*, 2008; Thompson *et al.*, 2008). However, the problems of

395 autocorrelation in evaluation models are rarely tested in transfer functions inferred from  
396 pollen data (Fr chet te *et al.*, 2008; Cao *et al.*, 2014; Tian Fang *et al.*, 2014), although these  
397 analyses are essential to obtain a robust transfer function.

398 Therefore to check if spatial autocorrelation affects the western Patagonia training set we have  
399 used the graphical method developed by Telford and Birks (2009). We compare the  
400 performance of the WA-PLS and MAT as the training set size is reduced by deleting sites at  
401 random, and by deleting sites geographically and environmentally close to the test site in  
402 cross-validation (Fig. S3). In the case of autocorrelation, deleting geographically close sites  
403 will preferentially delete the best analogues, and worsen the performance statistics more than  
404 random deletion. If the observations are independent, deleting a given proportion of them  
405 should have the same effect regardless of how they are selected (Telford and Birks, 2009).  
406 Our results suggest that the  $r^2$  from deleting of geographical neighbourhood sites closely  
407 follow the  $r^2$  from deleting the environmental neighbourhood sites indicating that  $P_{SUM}$  and  
408  $T_{WIN}$  are influenced by autocorrelation. The  $r^2$  scores strongly decrease after 40 km for  $P_{SUM}$   
409 and after 80 km for  $T_{WIN}$  and suggest that  $T_{WIN}$  seems to be less affected by autocorrelation  
410 than  $P_{SUM}$ . This strong  $r^2$  decrease shows that if a large amount of sites are deleted from the  
411 training set, the transfer functions are strongly affected by a lack of sample. This highlight the  
412 limited size of our training set from a region characterized by a complex environmental and  
413 vegetation gradient. In that case an enlarged dataset would be necessary to more rigorously  
414 perform model cross-validation and to address more fully these problems of spatial  
415 autocorrelation. However, another way to check the reliability of our models is to apply it to  
416 fossil pollen data and to compare the signal with independent proxies.

417

### 418 **4.3. Application of WA-PLS and the MAT to fossil pollen records**



419 Here we applied the WA-PLS and the MAT to two oceanic pollen records, core MD07-3088  
420 located at 46°S off Taitao Peninsula and core MD07-3104 located at 41°S in Reloncaví Fjord  
421 (Figs. 1 and 6). Spanning the last deglaciation and the Holocene, pollen data from core  
422 MD07-3088 illustrate the development of the North Patagonian Rainforest, which is  
423 interrupted by an expansion of Magellanic Moorland during the Antarctic Cold Reversal  
424 (ACR) (Montade *et al.*, 2013). Located further north, the core MD07-3104 shows  
425 compositional changes of temperate rainforest indicating warm and dry conditions during the  
426 beginning of the Holocene and more climate variability from the mid-Holocene associated  
427 with a cooling trend and with an increase of precipitation (Montade *et al.*, 2012). Although  
428 the climate reconstructions based on both models are consistent, the minor fluctuations  
429 indicated by the MAT do not evidence significant climate changes. As previously mentioned,  
430 this confirms that the MAT seems less appropriate than the WA-PLS to provide reliable  
431 climate reconstructions according to our modern pollen-climate dataset. For that reason, the  
432 climate reconstructions discussed below are based on the WA-PLS results.

433 Before 18 kyr, results obtained from core MD07-3088 at 46°S indicate lower values than  
434 modern ones for  $P_{SUM}$  (400-300 mm) and  $T_{WIN}$  (ca. 3°C). However, before 18 kyr, these  
435 results must be taken with caution given that during the late glacial, the pollen signal is  
436 characterized by low pollen concentrations reflecting reduced or absent vegetation on the  
437 adjacent land areas at a time, and the potential for non-analogue vegetation communities to be  
438 present during the glacial and post-glacial transition, when glaciers were greatly expanded  
439 compared to the present (Montade *et al.*, 2013). Under these conditions an overrepresentation  
440 of high producers of pollen such as *Nothofagus* trees was observed, which prevents local  
441 vegetation reconstructions and which is likely to bias our climate reconstructions at that time.  
442 From 18-17.5 kyr, a slight warming trend of 0.5°C is recorded, contemporaneous of the  
443 beginning of the deglaciation evidenced by the  $\delta D$  variations of EPICA Dome C ice core (Fig.

444 6d). Such a trend occurs simultaneously with the development of vegetation following the  
445 retreat of glaciers recorded in the region (Bennett *et al.*, 2000; Haberle and Bennett, 2004).  
446 Recorded from the same core, the beginning of the last deglaciation is also well evidenced by  
447 the increase of summer sea surface temperature (SSTs, Fig. 6c) reconstructed from  
448 planktonic foraminifera assemblages (Siani *et al.*, 2013). The strongest change evidenced by  
449 our climate reconstruction correspond to a rapid  $P_{SUM}$  increase starting at 14.5 kyr (ACR) with  
450 maximum values between 800 and 1000 mm. High  $P_{SUM}$  values persist up to the end of the  
451 Younger Dryas (YD) period (Fig. 6c). Simultaneously, we observe a progressive  $T_{WIN}$   
452 increase of ca. 2°C while for the SSTs, values stop to increase during the ACR then decrease  
453 of 1°C at 13 kyr before to reach maxima after the YD. This strong precipitation increase  
454 characterised by very high values suggests an intensification of the SWW during the ACR and  
455 the YD. Already recorded by previous studies from western Patagonia, this abrupt change was  
456 interpreted as a northward shift of the SWW belt (García *et al.*, 2012; Moreno *et al.*, 2012;  
457 Montade *et al.*, 2015). Today, latitudes under the core of the SWW belt where rainfalls are  
458 very high, the temperature seasonality is the lowest of western Patagonia and, because of  
459 strong ocean influence, temperature values remain always positive at low elevation.  
460 Consequently, after the last glacial conditions, such an intensification of SWW and  
461 precipitation would have reduced the temperature seasonality inducing a milder summer and  
462 winter temperature. This scenario might explain the observed  $T_{WIN}$  increase by our  
463 reconstruction. Based on this result, glacier advances evidenced in western Patagonia during  
464 the ACR and the YD might be more related to hydrological changes than to a strong cooling  
465 (Moreno *et al.*, 2009; García *et al.*, 2012; Glasser *et al.*, 2012). However, additional  
466 quantitative climate reconstructions are necessary to test this hypothesis.

467 After the YD,  $P_{SUM}$  reconstructed from core MD07-3088 decrease progressively to reach  
468 present-day values between 400 and 500 mm (Fig. 6a).  $T_{WIN}$  values (ca. 6°C) are maxima

469 during the early Holocene, before they slightly decrease and fluctuate between 5 and 6°C,  
470 close to modern values (Fig. 6c). This moderate change in comparison with the last  
471 deglaciation are consistent with past vegetation dynamics recorded from the same latitude  
472 showing that the North Patagonian Rainforest rapidly reaches its modern composition during  
473 the early Holocene (Bennett *et al.*, 2000). On the other hand, the core MD07-3104 indicates a  
474 stronger climate variability during the Holocene. After reaching their maxima after the YD,  
475  $P_{SUM}$  and  $T_{WIN}$  decrease from 500 to 350 mm and from 11 to 8.5°C from the early to the mid-  
476 Holocene (Figs. 6a and c). Then from 6 kyr,  $P_{SUM}$  and  $T_{WIN}$  fluctuate around 400 mm and 9°C  
477 before a slight decrease during the late Holocene to reach values close to the modern  
478 conditions. The climate variability reconstructed from core MD07-3104 is compared with a  
479 pollen index calculated from Lago Condorito located at ca. 30 km from the oceanic core  
480 (Moreno, 2004; Moreno *et al.*, 2010). Based on the normalized ratio between *Eucryphia-*  
481 *Caldcluvia* and *Podocarpus*, positive values of this index reflect a warm-temperate,  
482 seasonally dry climate with reduced SWW and negative values indicate cool-temperate and/or  
483 wet conditions with enhanced SWW. While our reconstruction indicates that  $T_{WIN}$  increase is  
484 associated with  $P_{SUM}$  increase, the pollen index indicates warm-temperate conditions under  
485 low precipitation (Fig. 6). This difference might be related to a different sensitivity of  
486 seasonality between the pollen index and our reconstructed  $T_{WIN}$ . On the other hand,  
487 comparison of  $P_{SUM}$  curve and the index reveals the same trend. Although a short time lag is  
488 observed, which is certainly related to a problem of marine age reservoir from the oceanic  
489 core (Montade *et al.*, 2012), our  $P_{SUM}$  reconstruction supports the known dynamic of  
490 precipitation and SWW changes in the region. Southward at 46°S, such changes are not  
491 recorded by our climate reconstruction and by vegetation changes (Montade *et al.*, 2013).  
492 Today the northern Patagonia at 41°S is characterized by a seasonally dry climate directly  
493 connected with a strong seasonality of SWW intensity. In comparison, the location of core

494 MD07-3088 closer to the position of the core of SWW already since the early Holocene,  
495 under the persistent influence of the SWW, rainfalls are strong all over the year.  
496 Consequently, this might explain why hydrological changes related to SWW changes would  
497 have more impacted the northern Patagonia during the Holocene.

498

## 499 **Conclusions**

500 To conclude, although based on different depositional environments (soil, lake and ocean),  
501 our modern pollen dataset (183 samples) from western Patagonia reflects the main vegetation  
502 types distributed along the latitudinal and the altitudinal gradient. Investigating the modern  
503 pollen-vegetation-climate relationships, we further demonstrate that the major vegetation  
504 distribution reflected by pollen assemblages is mainly controlled by two parameters:  $P_{SUM}$  and  
505  $T_{WIN}$ . Characterized by a southward  $T_{WIN}$  decrease and a southward  $P_{SUM}$  increase, these two  
506 parameters represent the main climatic limiting factor in western Patagonia controlling the  
507 latitudinal distribution of the vegetation. Based on the modern pollen dataset, we then  
508 analysed and compared the performance of two standard methods: the MAT and the WA-  
509 PLS. They adequately model taxa and their environments; however our results also reveal that  
510 the WA-PLS is more suitable than the MAT which suffers of a lack of modern pollen samples  
511 to perform reliable climate reconstructions. Using two oceanic cores from northern Patagonia  
512 at 41°S and 46°S we finally proceeded to reconstructions of  $P_{SUM}$  and  $T_{WIN}$  values during the  
513 late Glacial and the Holocene. The most important climate change occurred during ACR and  
514 YD where  $P_{SUM}$  reach the double amount of modern values related to an enhanced SWW.  
515 Although our results show several methodological limitations (mainly by using oceanic and  
516 terrestrial samples together), our climate reconstructions, consistent with the regional climate  
517 changes, illustrate the potential to develop quantitative methods in western Patagonia.  
518 Representing one of the parts of South America with the most pollen records, additional

519 quantitative climate reconstructions have to be performed to improve our understanding of  
520 climate dynamic at a regional scale. Furthermore, the modern pollen dataset still needs to be  
521 enlarged, to reduce uncertainties of climate reconstructions.

522

### 523 **Acknowledgements**

524 V.M. benefited from a postdoctoral position funded by Ecole Pratique des Hautes Etudes at  
525 Institut des Sciences de l'Evolution de Montpellier (ISEM) and Deutsche  
526 Forschungsgemeinschaft at Department of Palynology and Climate Dynamics from the  
527 University of Goettingen. We thank Vera Markgraf for sharing pollen data and for helpful  
528 comments on the first version of the manuscript. We also thank Elisabeth Michel and  
529 Giuseppe Siani for sharing data concerning the oceanic core MD07-3088. Finally we are  
530 particularly grateful from the very constructive comments from two anonymous referees  
531 greatly improving this manuscript. This is an ISEM contribution n°XX.

532

### 533 **References**

- 534 Anderson RF, Ali S, Bradtmiller LI, Nielsen SHH, Fleisher MQ, Anderson BE, Burckle LH.  
535 2009. Wind-Driven Upwelling in the Southern Ocean and the Deglacial Rise in  
536 Atmospheric CO<sub>2</sub>. *Science* **323**: 1443–1448.
- 537 Bennett KD, Haberle SG, Lumley SH. 2000. The Last Glacial-Holocene Transition in  
538 Southern Chile. *Science* **290**: 325–328.
- 539 ter Braak CJF, Juggins S. 1993. Weighted averaging partial least squares regression (WA-  
540 PLS): an improved method for reconstructing environmental variables from species  
541 assemblages. *Hydrobiologia* **269–270**: 485–502.

542 Brewer S, Guiot J, Barboni D. 2013. POLLEN METHODS AND STUDIES | Use of Pollen as  
543 Climate Proxies. In *Encyclopedia of Quaternary Science (Second Edition)*, Elias SA,  
544 Mock CJ (eds). Elsevier: Amsterdam; 805–815.

545 Cao X, Herzschuh U, Telford RJ, Ni J. 2014. A modern pollen–climate dataset from China  
546 and Mongolia: Assessing its potential for climate reconstruction. *Review of*  
547 *Palaeobotany and Palynology* **211**: 87–96.

548 Flantua SGA, Hooghiemstra H, Grimm EC, Behling H, Bush MB, González-Arango C,  
549 Gosling WD, Ledru M-P, Lozano-García S, Maldonado A, Prieto AR, Rull V, Van  
550 Boxel JH. 2015. Updated site compilation of the Latin American Pollen Database.  
551 *Review of Palaeobotany and Palynology* **223**: 104–115.

552 Francois J-P. 2014. *Postglacial paleoenvironmental history of the Southern Patagonian*  
553 *Fjords at 53°S*. PhD thesis. Universität zu Köln.

554 Fréchette B, de Vernal A, Guiot J, Wolfe AP, Miller GH, Fredskild B, Kerwin MW, Richard  
555 PJH. 2008. Methodological basis for quantitative reconstruction of air temperature and  
556 sunshine from pollen assemblages in Arctic Canada and Greenland. *Quaternary*  
557 *Science Reviews* **27**: 1197–1216.

558 Gajardo R. 1994. *La vegetación natural de Chile : clasificación y distribución geográfica*.  
559 Santiago.

560 García JL, Kaplan MR, Hall BL, Schaefer JM, Vega RM, Schwartz R, Finkel R. 2012.  
561 Glacier expansion in southern Patagonia throughout the Antarctic cold reversal.  
562 *Geology* **40**: 859–862.

563 Garreaud R, Lopez P, Minvielle M, Rojas M. 2013. Large-Scale Control on the Patagonian  
564 Climate. *Journal of Climate* **26**: 215–230.

565 Garreaud RD, Vuille M, Compagnucci R, Marengo J. 2009. Present-day South American  
566 climate. *Palaeogeography, Palaeoclimatology, Palaeoecology* **281**: 180–195.

567 Glasser NF, Harrison S, Schnabel C, Fabel D, Jansson KN. 2012. Younger Dryas and early  
568 Holocene age glacier advances in Patagonia. *Quaternary Science Reviews* **58**: 7–17.

569 Grieser J, Giommes R, Bernardi M. 2006. New\_LocClim - the Local Climate Estimator of  
570 FAO. *Geophysical Research Abstracts* **8**: 08305.

571 Guiot J. 1990. Methodology of the last climatic cycle reconstruction in France from pollen  
572 data. *Palaeogeography, Palaeoclimatology, Palaeoecology* **80**: 49–69.

573 Guiot J, de Vernal A. 2007. Chapter Thirteen Transfer Functions: Methods for Quantitative  
574 Paleoceanography Based on Microfossils. In *Developments in Marine Geology*,  
575 Hillaire–Marcel C, de Vernal A. (eds). Elsevier: Amsterdam; 523–563.

576 Haberle SG, Bennett KD. 2001. Modern pollen rain and lake mud-water interface  
577 geochemistry along environmental gradients in southern Chile. *Review of*  
578 *Palaeobotany and Palynology* **117**: 93–107.

579 Haberle SG, Bennett KD. 2004. Postglacial formation and dynamics of North Patagonian  
580 Rainforest in the Chonos Archipelago, Southern Chile. *Quaternary Science Reviews*  
581 **23**: 2433–2452.

582 Harrison SP, Bartlein PJ, Prentice IC. 2016. What have we learnt from palaeoclimate  
583 simulations? *Journal of Quaternary Science* **31**: 363–385.

584 Heusser CJ. 2003. *Ice age Southern Andes - A chronicle of paleoecological events*. Elsevier:  
585 Amsterdam.

586 Hijmans RJ, Cameron SE, Parra JL, Jones PG, Jarvis A. 2005. Very high resolution  
587 interpolated climate surfaces for global land areas. *International Journal of*  
588 *Climatology* **25**: 1965–1978.

589 Juggins PS. 2015. rioja: Analysis of Quaternary Science Data. <http://eprints.ncl.ac.uk>.

590 Kilian R, Lamy F. 2012. A review of Glacial and Holocene paleoclimate records from  
591 southernmost Patagonia (49–55°S). *Quaternary Science Reviews* **53**: 1–23.

592 Lemieux-Dudon B, Blayo E, Petit J-R, Waelbroeck C, Svensson A, Ritz C, Barnola J-M,  
593 Narcisi BM, Parrenin F. 2010. Consistent dating for Antarctic and Greenland ice  
594 cores. *Quaternary Science Reviews* **29**: 8–20.

595 Luebert F, Plischoff P. 2004. *Classification de pisos de vegetacion y analisis de*  
596 *representatividad ecologica de areas propuesta para la proteccion en la ecoregion*  
597 *valdivia*. Santiago.

598 Mancini MV, de Porras ME, Bamonte FP. 2012. Southernmost South America Steppes:  
599 vegetation and its modern pollen-assemblages representation. In *Steppe Ecosystem*  
600 *Dynamics, Land Use and Conservation*, Germano D (ed). Nova Science Publishers:  
601 New York; 141–156.

602 Markgraf V, Webb RS, Anderson KH, Anderson L. 2002. Modern pollen/climate calibration  
603 for southern South America. *Palaeogeography, Palaeoclimatology, Palaeoecology*  
604 **181**: 375–397.

605 Mauri A, Davis BAS, Collins PM, Kaplan JO. 2015. The climate of Europe during the  
606 Holocene: a gridded pollen-based reconstruction and its multi-proxy evaluation.  
607 *Quaternary Science Reviews* **112**: 109–127.

608 Montade V, Combourieu-Nebout N, Chapron E, Mulsow S, Abarzúa AM, Debret M, Foucher  
609 A, Desmet M, Winiarski T, Kissel C. 2012. Regional vegetation and climate changes  
610 during the last 13 kyr from a marine pollen record in Seno Reloncaví, southern Chile.  
611 *Review of Palaeobotany and Palynology* **181**: 11–21.

612 Montade V, Combourieu-Nebout N, Kissel C, Haberle SG, Siani G, Michel E. 2013.  
613 Vegetation and climate changes during the last 22,000 yr from a marine core near  
614 Taitao Peninsula, southern Chile. *Palaeogeography, Palaeoclimatology,*  
615 *Palaeoecology* **369**: 335–348.



616 Montade V, Combourieu-Nebout N, Kissel C, Mulrow S. 2011. Pollen distribution in marine  
617 surface sediments from Chilean Patagonia. *Marine Geology* **282**: 161–168.

618 Montade V, Kageyama M, Combourieu-Nebout N, Ledru M-P, Michel E, Siani G, Kissel C.  
619 2015. Teleconnection between the Intertropical Convergence Zone and southern  
620 westerly winds throughout the last deglaciation. *Geology* **43**: 735–738.

621 Moreno PI. 2004. Millennial-scale climate variability in northwest Patagonia over the last 15  
622 000 yr. *Journal of Quaternary Science* **19**: 35–47.

623 Moreno PI, Francois JP, Moy CM, Villa-Martínez R. 2010. Covariability of the Southern  
624 Westerlies and atmospheric CO<sub>2</sub> during the Holocene. *Geology* **38**: 727–730.

625 Moreno PI, Kaplan MR, Francois JP, Villa-Martinez R, Moy CM, Stern CR, Kubik PW.  
626 2009. Renewed glacial activity during the Antarctic cold reversal and persistence of  
627 cold conditions until 11.5 ka in southwestern Patagonia. *Geology* **37**: 375–378.

628 Moreno PI, Vilanova I, Villa-Martínez R, Garreaud RD, Rojas M, De Pol-Holz R. 2014.  
629 Southern Annular Mode-like changes in southwestern Patagonia at centennial  
630 timescales over the last three millennia. *Nature Communications* **5**: 4375.

631 Moreno PI, Villa-Martínez R, Cárdenas ML, Sagredo EA. 2012. Deglacial changes of the  
632 southern margin of the southern westerly winds revealed by terrestrial records from  
633 SW Patagonia (52°S). *Quaternary Science Reviews* **41**: 1–21.

634 Ortega-Rosas CI, Peñalba MC, Guiot J. 2016. The Lateglacial interstadial at the southeastern  
635 limit of the Sonoran Desert, Mexico: vegetation and climate reconstruction based on  
636 pollen sequences from Ciénega San Marcial and comparison with the subrecent  
637 record. *Boreas* **45**: 773–789.

638 Paez MM, Schäbitz F, Stutz S. 2001. Modern pollen–vegetation and isopoll maps in southern  
639 Argentina. *Journal of Biogeography* **28**: 997–1021.

640 Peyron O, Goring S, Dormoy I, Kotthoff U, Pross J, de Beaulieu J-L, Drescher-Schneider R,  
641 Vanni re B, Magny M. 2011. Holocene seasonality changes in the central  
642 Mediterranean region reconstructed from the pollen sequences of Lake Accesa (Italy)  
643 and Tenaghi Philippon (Greece). *The Holocene* **21**: 131–146.

644 Prentice IC. 1980. Multidimensional scaling as a research tool in quaternary palynology: A  
645 review of theory and methods. *Review of Palaeobotany and Palynology* **31**: 71–104.

646 Sch bitz F, Wille M, Francois J-P, Haberzettl T, Quintana F, Mayr C, L ucke A, Ohlendorf C,  
647 Mancini V, Paez MM, Prieto AR, Zolitschka B. 2013. Reconstruction of  
648 palaeoprecipitation based on pollen transfer functions – the record of the last 16 ka  
649 from Laguna Potrok Aike, southern Patagonia. *Quaternary Science Reviews* **71**: 175–  
650 190.

651 Schmith sen J. 1956. Die r umliche Ordnung der chilenischen Vegetation. *Bonner*  
652 *Geographische Abhandlungen* **17**: 1–86.

653 Siani G, Michel E, De Pol-Holz R, DeVries T, Lamy F, Carel M, Isguder G, Dewilde F,  
654 Lourantou A. 2013. Carbon isotope records reveal precise timing of enhanced  
655 Southern Ocean upwelling during the last deglaciation. *Nature Communications* **4**.

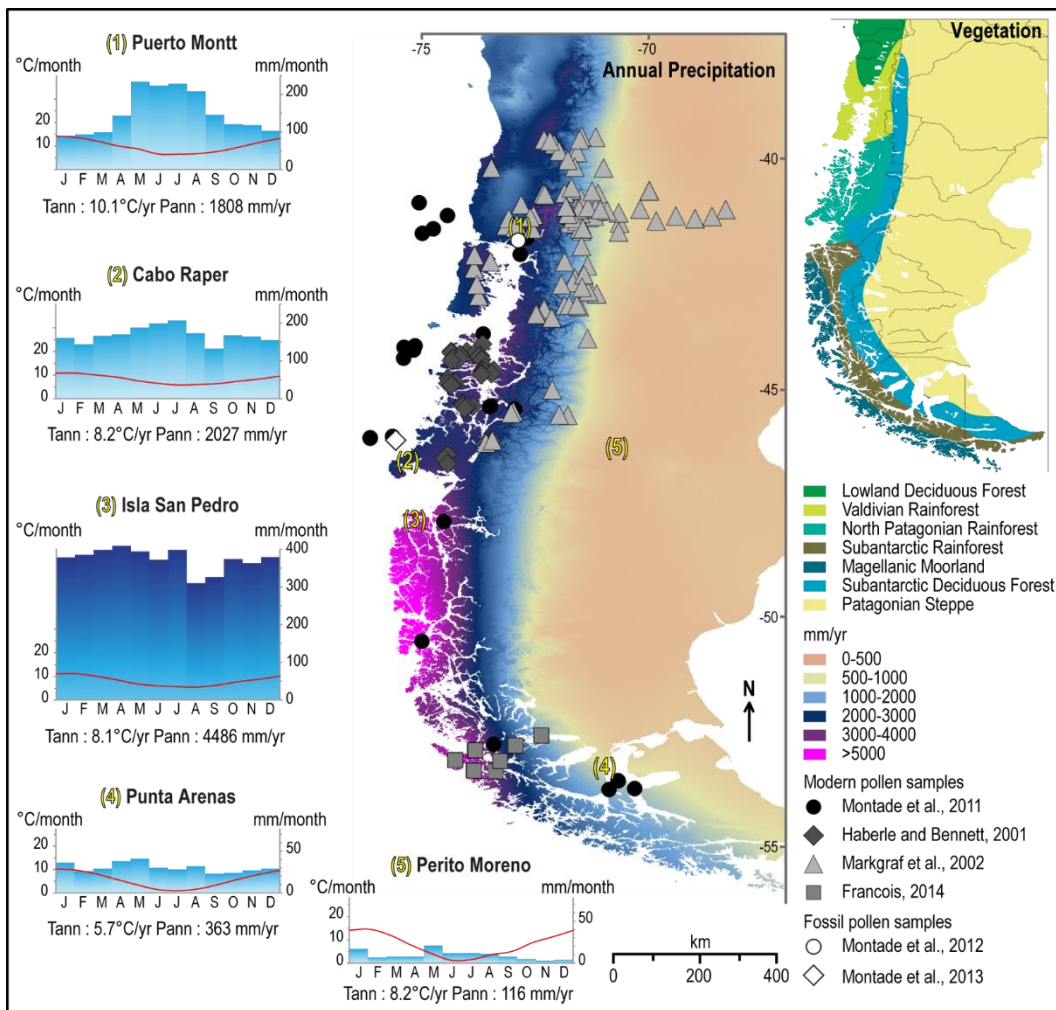
656 Telford RJ. 2015. *palaeoSig: Significance Tests for Palaeoenvironmental Reconstructions*.

657 Telford RJ, Birks HJB. 2005. The secret assumption of transfer functions: problems with  
658 spatial autocorrelation in evaluating model performance. *Quaternary Science Reviews*  
659 **24**: 2173–2179.

660 Telford RJ, Birks HJB. 2009. Evaluation of transfer functions in spatially structured  
661 environments. *Quaternary Science Reviews* **28**: 1309–1316.

662 Thompson RS, Anderson KH, Bartlein PJ. 2008. Quantitative estimation of bioclimatic  
663 parameters from presence/absence vegetation data in North America by the modern  
664 analog technique. *Quaternary Science Reviews* **27**: 1234–1254.

- 665 Tian F, Herzschuh U, Telford RJ, Mischke S, Van der Meeren T, Krenzel M, Richardson J.  
666 2014. A modern pollen–climate calibration set from central-western Mongolia and its  
667 application to a late glacial–Holocene record. *Journal of Biogeography* **41**: 1909–  
668 1922.
- 669 Toggweiler JR, Russell JL, Carson SR. 2006. Midlatitude westerlies, atmospheric CO<sub>2</sub>, and  
670 climate change during the ice ages. *Paleoceanography* **21**: 1–15.
- 671 Tonello MS, Mancini MV, Seppä H. 2009. Quantitative reconstruction of Holocene  
672 precipitation changes in southern Patagonia. *Quaternary Research* **72**: 410–420.
- 673 Tonello MS, Prieto AR. 2008. Modern vegetation–pollen–climate relationships for the Pampa  
674 grasslands of Argentina. *Journal of Biogeography* **35**: 926–938.
- 675 Villa-Martínez R, Moreno PI, Valenzuela MA. 2012. Deglacial and postglacial vegetation  
676 changes on the eastern slopes of the central Patagonian Andes (47°S). *Quaternary*  
677 *Science Reviews* **32**: 86–99.
- 678
- 679



681

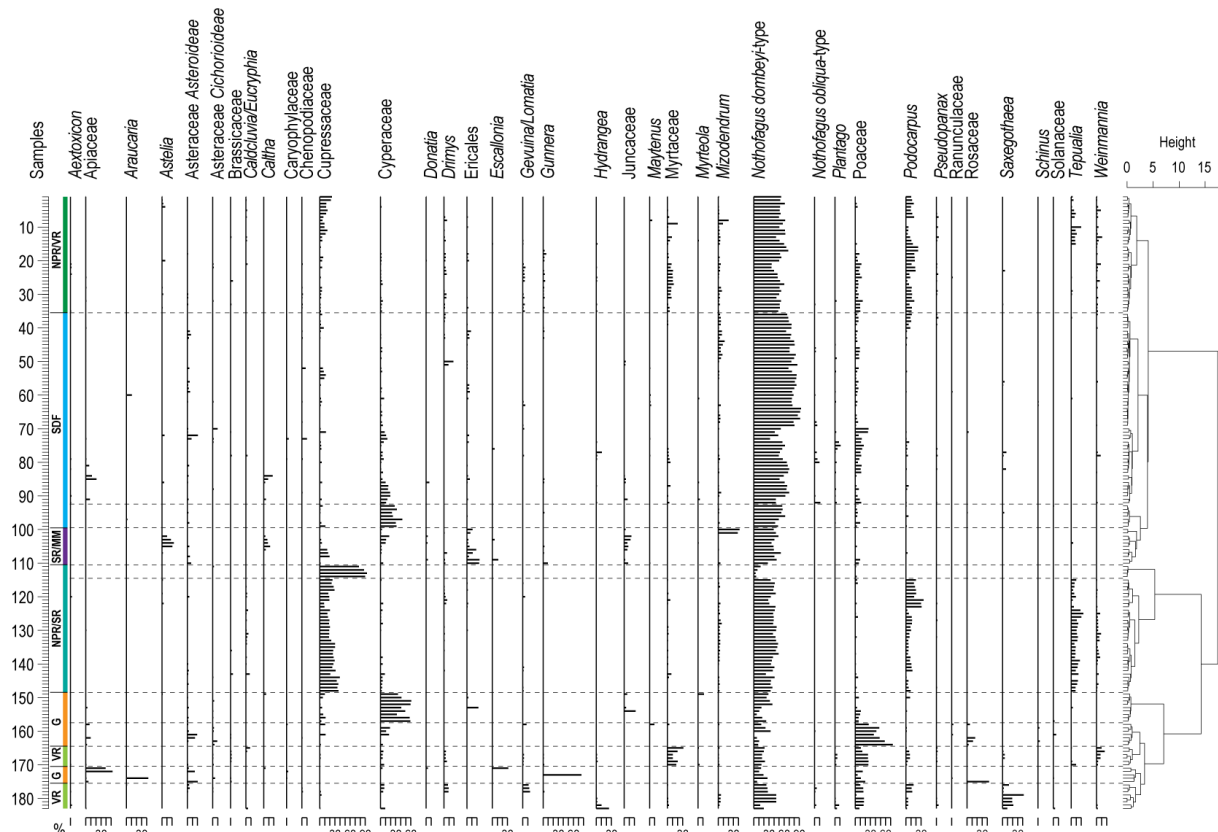
682 **Figure 1.** Climate and vegetation maps from Patagonia with location of modern samples and

683 fossil pollen records used in this study. Precipitation data were obtained from WorldClim

684 database (Hijmans *et al.*, 2005), climatographs were performed using data from

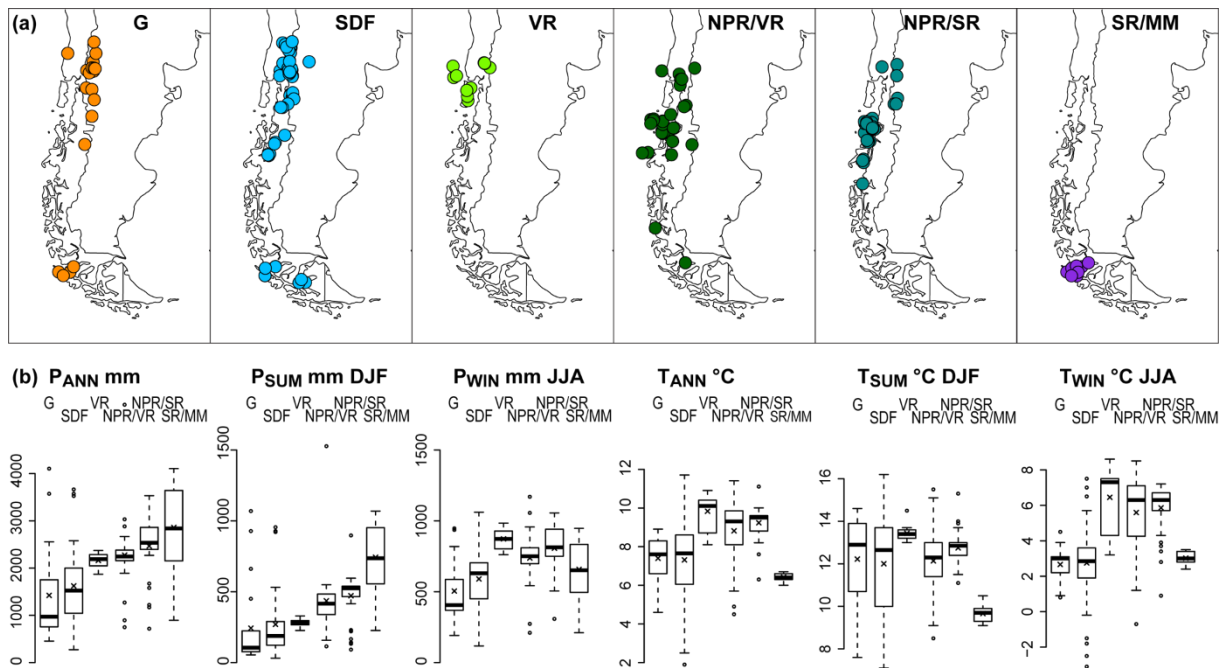
685 meteorological stations (New\_LocClim\_1.10 software; Grieser *et al.*, 2006) and vegetation

686 distribution is adapted from Schimithüsen (1956).



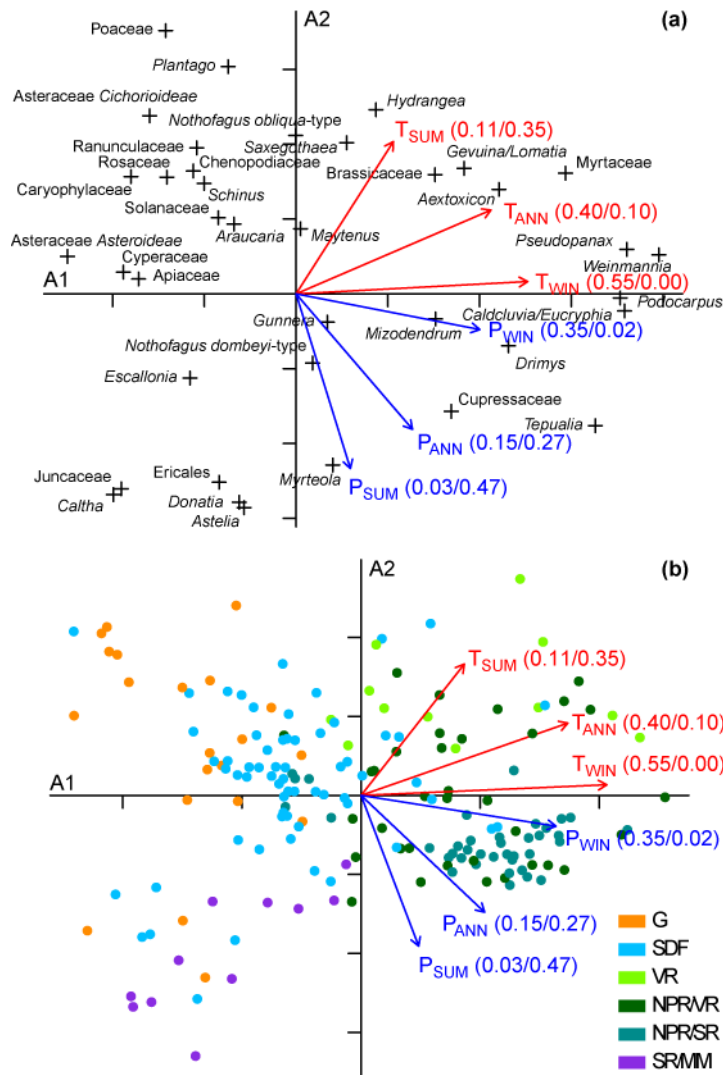
688 **Figure 2.** Pollen diagram of the 183 modern pollen samples from western Patagonia showing  
 689 the main pollen taxa. Ordination of modern pollen samples with pollen zones have been made  
 690 using a cluster analysis based on chord distance. According to the pollen assemblages of each  
 691 zone, six vegetation groups were identified: Grassland (G), Subantarctic Deciduous Forest  
 692 (SDF), Valdivian Rainforest (VR), North Patagonian/Valdivian Rainforest (NPR/VR), North  
 693 Patagonian/Subantarctic Rainforest (NPR/SR), Subantarctic Rainforest/Magellanic Moorland  
 694 (SR/MM).

696



697  
 698 **Figure 3.** Distribution maps (a) of the 183 surface samples according to their respective  
 699 vegetation groups attributed from pollen assemblages: Grassland (G), Subantarctic Deciduous  
 700 Forest (SDF), Valdivian Rainforest (VR), North Patagonian/Valdivian Rainforest (NPR/VR),  
 701 North Patagonian/Subantarctic Rainforest (NPR/SR), Subantarctic Rainforest/Magellanic  
 702 Moorland (SR/MM). Boxplots (b) represent the main climate parameters of present-day  
 703 climate as they relate to the different vegetation groups:  $P_{ANN}$  and  $T_{ANN}$  correspond  
 704 respectively to the annual precipitation and the mean annual temperature,  $P_{SUM}$  and  $P_{WIN}$   
 705 correspond respectively to the precipitation sum of December-January-February and June-  
 706 July-August,  $T_{SUM}$  and  $T_{WIN}$  correspond to mean temperature of the same months as  $P_{SUM}$  and  
 707  $P_{WIN}$ . The cross on each boxplot indicates the mean value for each climate parameter.

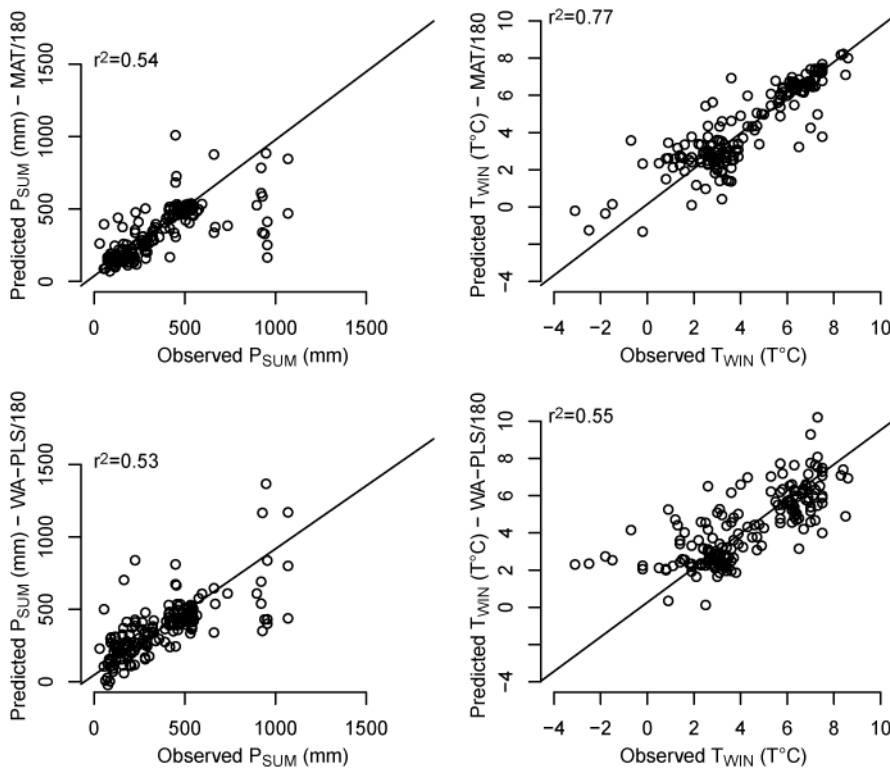
708



709

710 **Figure 4.** Bi-plot of the principal component analysis (PCA) with the 38 selected pollen taxa  
 711 (a) and the 183 selected modern pollen samples (b). Eigenvalues for the first and second axes  
 712 represent respectively 14% and 13% of the total variation. The arrows indicate the passive  
 713 climate parameter projected in the axes 1-2 bi-plot of the PCA with their respective  $r^2$ :  $P_{ANN}$   
 714 and  $T_{ANN}$  correspond respectively to the annual precipitation and the mean annual  
 715 temperature,  $P_{SUM}$  and  $P_{WIN}$  correspond respectively to the precipitation sum of December-  
 716 January-February and June-July-August,  $T_{SUM}$  and  $T_{WIN}$  correspond to mean temperature of  
 717 the same months as  $P_{SUM}$  and  $P_{WIN}$ . Grassland (G), Subantarctic Deciduous Forest (SDF),  
 718 Valdivian Rainforest (VR), North Patagonian/Valdivian Rainforest (NPR/VR), North

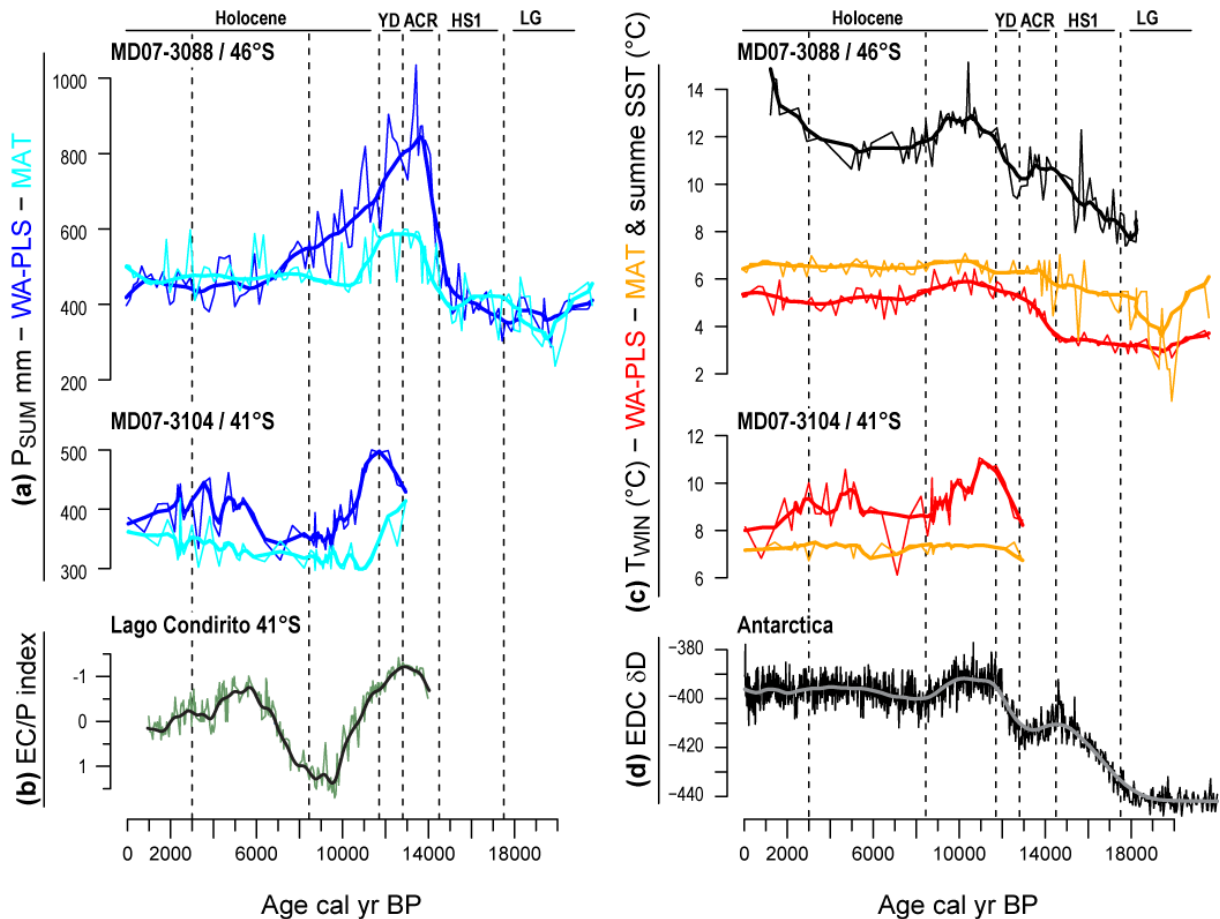
719 Patagonian/Subantarctic Rainforest (NPR/SR), Subantarctic Rainforest/Magellanic Moorland  
720 (SR/MM).



721  
722 **Figure 5.** Comparison of predicted versus observed P<sub>SUM</sub> (precipitation sum of December-  
723 January-February) and T<sub>WIN</sub> (mean temperature from June to August) performed on the 180  
724 samples including oceanic and terrestrial pollen data from western Patagonia (excluding three  
725 outliers) and using the Modern Analog Technique (MAT) and the Weighted Averaging Partial  
726 Least Squares (WA-PLS).

727





728  
 729 **Figure 6.** Climate reconstructions from core MD07-3088 and core MD07-3104 compared  
 730 with independent palaeoclimatic proxies. The  $P_{SUM}$  (precipitation sum of December-January-  
 731 February) and  $T_{WIN}$  (mean temperature from June to August) have been reconstructed using  
 732 the MAT (Modern Analog Technique) and the WA-PLS (Weighted Averaging Partial Least  
 733 Squares) with the pollen-climate training set of 180 samples. (a)  $P_{SUM}$  from core MD07-3088  
 734 and MD07-3104; (b) EC/P (*Eucryphia-Caldcluvia/Podocarpus*) index from Lago Condorito  
 735 (Moreno, 2004); (c) SSTs (Summer Sea Surface Temperatures) from core MD07-3088 based  
 736 on planktonic foraminifera assemblages (Siani *et al.*, 2013) with  $T_{WIN}$  from core MD07-3088  
 737 and MD07-3104; (d) Ice-core  $\delta D$  based on the age scale of Lemieux-Dudon *et al.* (2010). The  
 738 original data were fit with a cubic smoothing spline (bold lines). YD, Younger Dryas; ACR,  
 739 Antarctic Cold Reversal; HS1, Heinrich Stadial 1; LGM, Last Glacial Maximum.

741 **Table 1.** Performance of the Weighted Averaging Partial Least Squares (WA-PLS) and the  
742 Modern Analog Technique (MAT) based on leave-one-out cross-validation with 183 and 180  
743 samples including oceanic and terrestrial pollen data from western Patagonia ( $P_{SUM}$ ,  
744 precipitation sum of December-January-February;  $T_{WIN}$ , mean temperature from June to  
745 August). The table indicate the best selected component for each parameter and cross-  
746 validation test.

747

Model	Component	Variables	Range	$r^2$	RMSEP	RMSEP % of gradient	Maximum Bias	Average Bias
MAT-183	-	$P_{SUM}$	31-1527 mm	0.49	180.8	12.1	1035	17.50
WA-PLS-183	2	$P_{SUM}$	31-1527 mm	0.44	193.3	12.9	925	2.62
MAT-183	-	$T_{WIN}$	-3.1-8.6 °C	0.77	1.1	20.3	2.1	2.08
WA-PLS-183	2	$T_{WIN}$	-3.1-8.6 °C	0.56	1.6	28.2	5.1	-0.05
MAT-180	-	$P_{SUM}$	31-1069 mm	0.54	162	15.6	446	17.31
WA-PLS-180	2	$P_{SUM}$	31-1069 mm	0.53	164	15.8	266	-0.28
MAT-180	-	$T_{WIN}$	-3.1-8.6 °C	0.77	1.1	20.4	2.1	-0.04
WA-PLS-180	2	$T_{WIN}$	-3.1-8.6 °C	0.55	1.6	28.5	5.1	-0.05

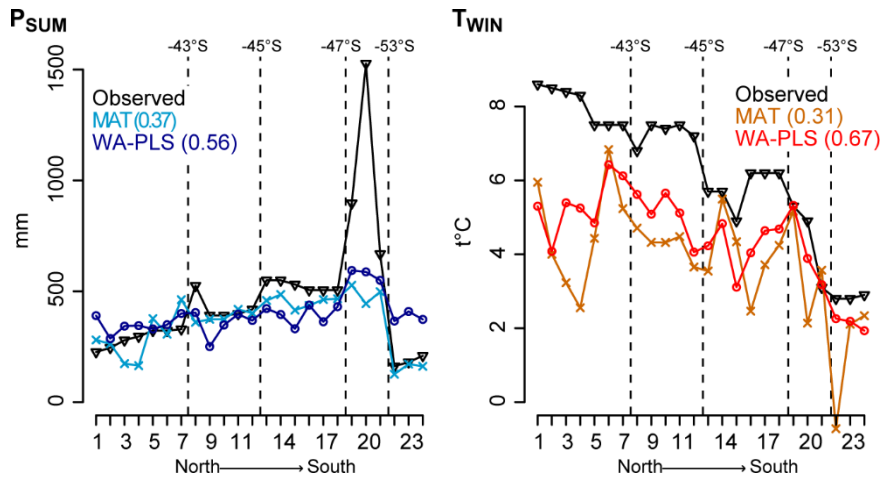
748

749

750 **Supporting Information**

751

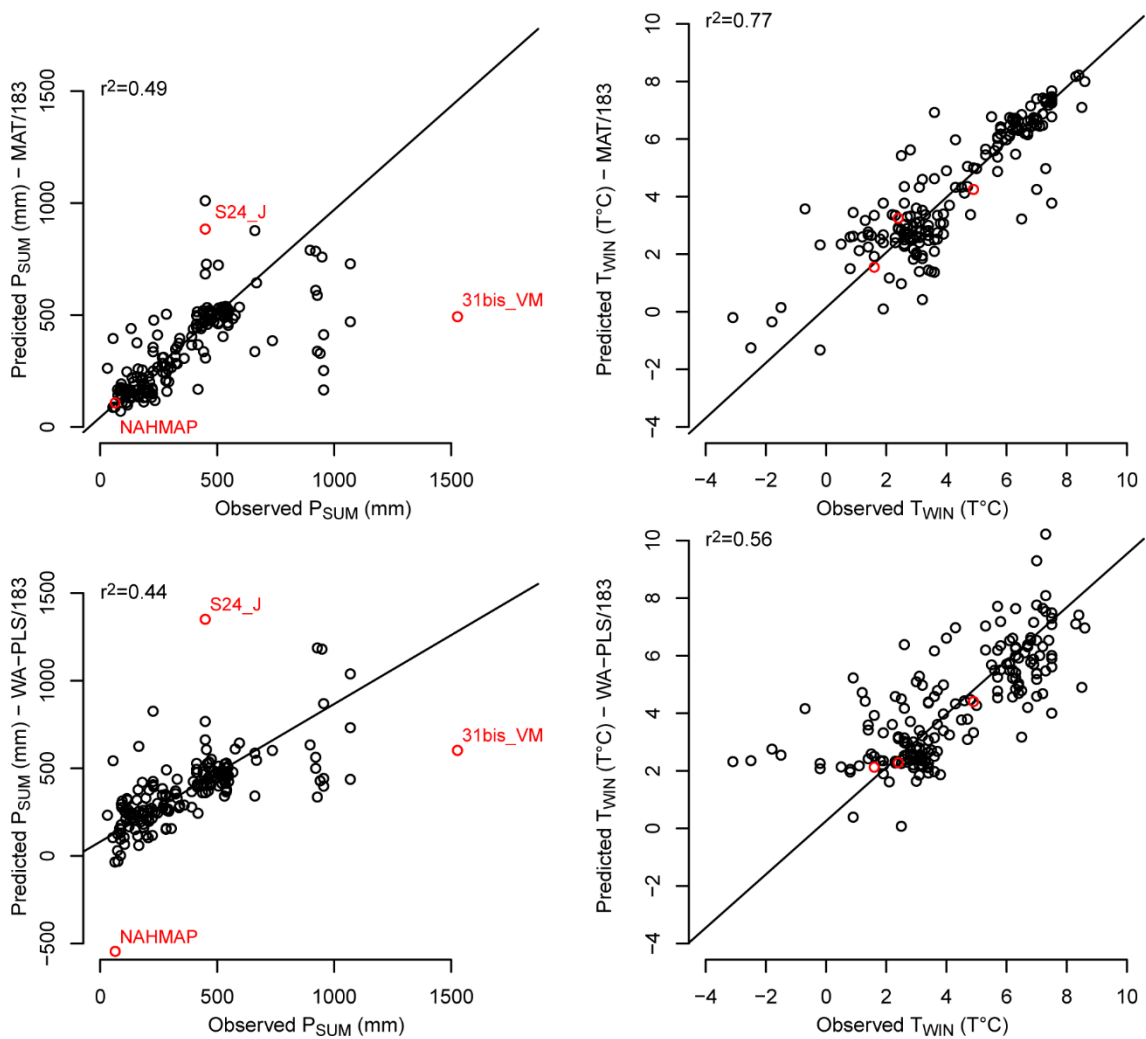
752 **Figure S1.** Comparison between observed and reconstructed present-day climate parameters  
753 performed on the 24 modern oceanic pollen samples with the terrestrial pollen dataset  
754 including 159 samples. The two climate parameters  $P_{SUM}$  (precipitation sum of December-  
755 January-February) and  $T_{WIN}$  (mean temperature from June to August) are indicated from north  
756 to south with their respective  $r^2$  between the observed and reconstructed values. MAT,  
757 Modern Analog Technique; WA-PLS, Weighted Averaging Partial Least Squares.



758

759

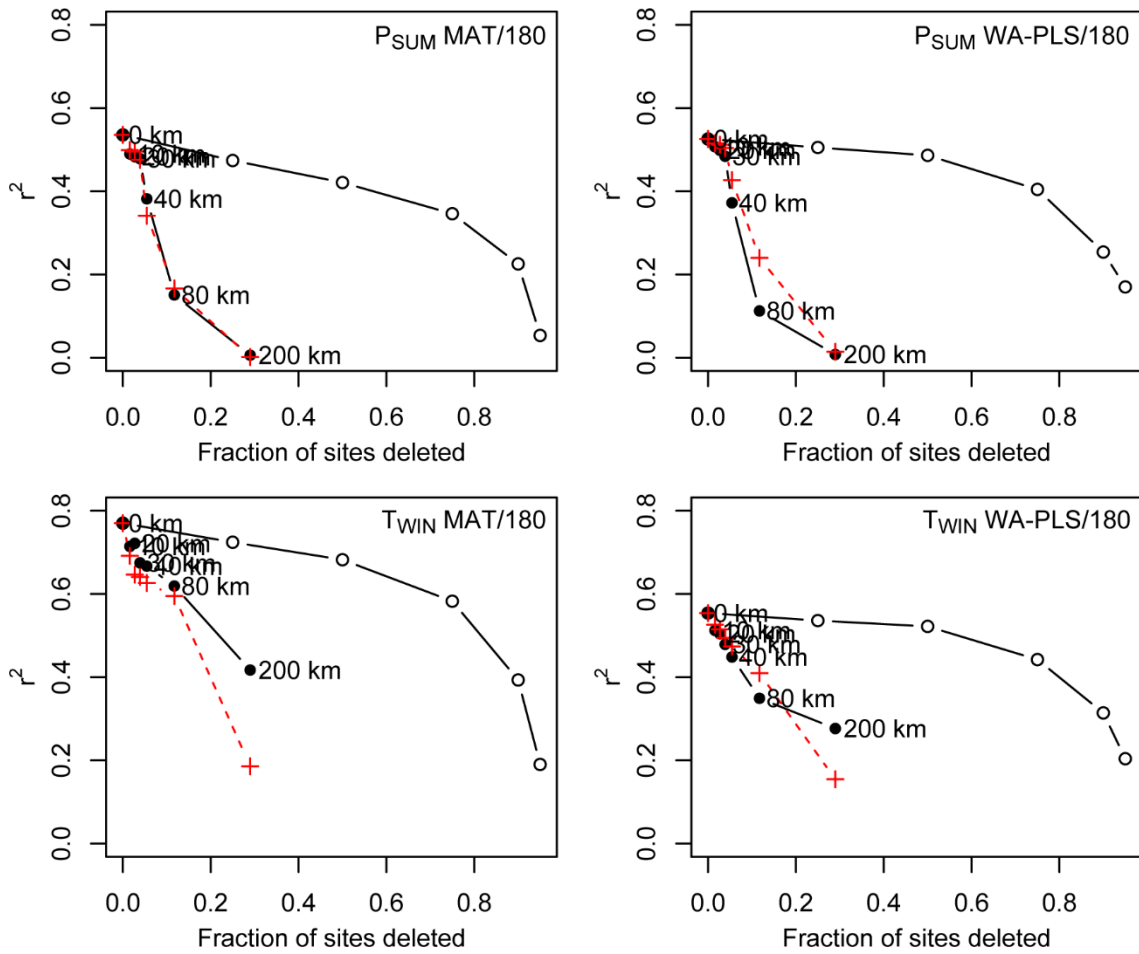
760 **Figure S2.** Comparison of predicted versus observed  $P_{SUM}$  (precipitation sum of December-  
 761 January-February) and  $T_{WIN}$  (mean temperature from June to August) performed on the 183  
 762 samples including oceanic and terrestrial pollen data from western Patagonia and using the  
 763 Modern Analog Technique (MAT) and the Weighted Averaging Partial Least Squares (WA-  
 764 PLS). Samples indicated in red correspond to the outliers identified from  $P_{SUM}$  and removed  
 765 of the second 180-training set.



766

767

768 **Figure S3.** Effect of transfer function  $r^2$  of deleting sites at random (mean of 10 trials; open  
769 circles) and from the geographical and environmental neighbourhood of the test site (filled  
770 circles and crosses) during cross-validation for the 180-training set.  $P_{SUM}$ , precipitation sum of  
771 December-January-February;  $T_{WIN}$ , mean temperature from June to August; MAT, Modern  
772 Analog Technique; WA-PLS, Weighted Averaging Partial Least Squares.



773

774

775 **Table S1.** List of the surface pollen samples from southern Patagonia according to their  
776 location (Long., east longitude and Lat., north latitude) and altitude (m asl). The column  
777 ‘code’ indicate the order of samples in the pollen diagram perform by the cluster analysis  
778 (samples without code correspond to samples excluded to perform statistical analyses). The  
779 type correspond to oceanic (O), soil (S) and lake (L) samples. Reference (Ref.) to publication  
780 1 (Montade *et al.*, 2011), 2 (Haberle and Bennett, 2001), 3 (Francois, 2014) and 4 (Markgraf  
781 *et al.*, 2002). Vegetation groups: Grassland (G), Subantarctic Deciduous Forest (SDF),  
782 Valdivian Rainforest (VR), North Patagonian/Valdivian Rainforest (NPR/VR), North  
783 Patagonian/Subantarctic Rainforest (NPR/SR), Subantarctic Rainforest/Magellanic Moorland  
784 (SR/MM), Indeterminate (Ind).

Name	Code	Type	Long.	Lat.	m asl	Ref.	Vegetation
7_VM	28	O	-76.1	-46.07	0	1	NPR/VR
8_VM	30	O	-76.1	-46.08	0	1	NPR/VR
11_VM	34	O	-75.37	-44.33	0	1	NPR/VR
12_VM	24	O	-75.36	-44.09	0	1	NPR/VR
13bis_VM	31	O	-75.15	-44.15	0	1	NPR/VR
14ter_VM	33	O	-74.41	-41.21	0	1	NPR/VR
15_VM	176	O	-75.03	-40.93	0	1	VR
16_VM	177	O	-74.96	-41.6	0	1	VR
17_VM	178	O	-74.72	-41.5	0	1	VR
18bis_VM	21	O	-72.78	-41.71	0	1	NPR/VR
19ter_VM	35	O	-72.67	-41.7	0	1	NPR/VR
20_VM	22	O	-72.82	-42.06	0	1	NPR/VR
21_VM	25	O	-75.12	-44.06	0	1	NPR/VR
22_VM	23	O	-73.63	-43.8	0	1	NPR/VR
23bis_VM	19	O	-73.47	-45.38	0	1	NPR/VR
24_VM	29	O	-73.49	-45.39	0	1	NPR/VR
26_VM	39	O	-72.94	-45.44	0	1	SDF
27_VM	18	O	-75.61	-46.04	0	1	NPR/VR
30_VM	122	O	-74.49	-47.9	0	1	NPR/SR
31bis_VM	20	O	-74.97	-50.52	0	1	NPR/VR
33_VM	107	O	-73.4	-52.77	0	1	SR/MM
36_VM	42	O	-70.88	-53.76	0	1	SDF
37_VM	43	O	-70.68	-53.57	0	1	SDF
38_VM	41	O	-70.32	-53.74	0	1	SDF
1_SH	132	L	-73.64	-44.02	25	2	NPR/SR
2_SH	10	L	-74.33	-44.18	75	2	NPR/VR
3_SH	131	L	-73.99	-44.18	30	2	NPR/SR

4_SH	13	L	-74.33	-44.21	75	2	NPR/VR
5_SH	136	L	-74.33	-44.21	75	2	NPR/SR
6_SH	11	L	-74.33	-44.21	75	2	NPR/VR
7_SH	127	L	-73.83	-44.24	50	2	NPR/SR
8_SH	145	L	-74.13	-44.25	49	2	NPR/SR
9_SH	128	L	-74.13	-44.26	47	2	NPR/SR
10_SH	138	L	-73.69	-44.27	75	2	NPR/SR
11_SH	133	L	-73.72	-44.29	75	2	NPR/SR
12_SH	125	L	-73.72	-44.29	75	2	NPR/SR
13_SH	124	L	-74.28	-44.33	10	2	NPR/SR
14_SH	129	L	-74.29	-44.33	10	2	NPR/SR
15_SH	146	L	-74.14	-44.33	25	2	NPR/SR
16_SH	134	L	-73.66	-44.36	50	2	NPR/SR
17_SH	137	L	-73.66	-44.36	50	2	NPR/SR
18_SH	135	L	-73.66	-44.36	50	2	NPR/SR
19_SH	12	L	-74.33	-44.38	125	2	NPR/VR
20_SH	139	L	-73.6	-44.52	76	2	NPR/SR
21_SH	14	L	-73.4	-44.59	20	2	NPR/VR
22_SH	115	L	-73.65	-44.59	30	2	NPR/SR
23_SH	147	L	-73.63	-44.6	30	2	NPR/SR
24_SH	140	L	-73.6	-44.63	20	2	NPR/SR
25_SH	126	L	-73.66	-44.66	400	2	NPR/SR
26_SH	130	L	-73.45	-44.67	25	2	NPR/SR
27_SH	3	L	-73.67	-44.69	750	2	NPR/VR
28_SH	4	L	-73.67	-44.69	770	2	NPR/VR
29_SH	1	L	-74.4	-44.76	25	2	NPR/VR
30_SH	5	L	-74.39	-44.78	25	2	NPR/VR
31_SH	6	L	-74.24	-44.86	75	2	NPR/VR
32_SH	119	L	-74.33	-44.88	25	2	NPR/SR
33_SH	7	L	-74.41	-44.88	25	2	NPR/VR
34_SH	2	L	-74.33	-44.92	75	2	NPR/VR
35_SH	148	L	-74.1	-45.33	25	2	NPR/SR
36_SH	116	L	-74.08	-45.33	125	2	NPR/SR
37_SH	117	L	-74.07	-45.37	25	2	NPR/SR
38_SH	120	L	-73.85	-45.38	25	2	NPR/SR
39_SH	141	L	-73.98	-45.39	85	2	NPR/SR
40_SH	142	L	-74.03	-45.43	25	2	NPR/SR
41_SH	36	L	-73.44	-46.14	120	2	SDF
42_SH	16	L	-73.57	-46.18	825	2	NPR/VR
43_SH	40	L	-73.58	-46.19	675	2	SDF
44_SH	37	L	-73.51	-46.23	75	2	SDF
45_SH	118	L	-74.41	-46.44	25	2	NPR/SR
46_SH	123	L	-74.49	-46.52	25	2	NPR/SR
47_SH	121	L	-74.41	-46.64	25	2	NPR/SR
S38_J	153	S	-74.24	-53.12	2	3	G
S39(2)_J	102	S	-74.24	-53.12	78	3	SR/MM

S39(1)_J	103	S	-74.24	-53.12	78	3	SR/MM
S32_J	171	S	-73.84	-53.34	378	3	G
S29_J	109	S	-73.83	-53.35	2	3	SR/MM
S31_J	72	S	-73.84	-53.34	324	3	SDF
S30_J	61	S	-73.83	-53.35	70	3	SDF
S28_J	50	S	-73.83	-53.35	12	3	SDF
S34_J	100	S	-73.36	-53.36	26	3	SR/MM
S16_J	84	S	-73.81	-52.9	290	3	SDF
S9_J	104	S	-73.8	-52.91	30	3	SR/MM
S21_J	91	S	-73.81	-52.9	256	3	SDF
S4_J	101	S	-73.8	-52.9	155	3	SR/MM
S36_J	149	S	-73.26	-53.14	6	3	G
S35_J	108	S	-73.26	-53.14	30	3	SR/MM
S25_J	85	S	-72.94	-52.81	411	3	SDF
S24_J	105	S	-72.93	-52.81	90	3	SR/MM
S26_J	106	S	-72.93	-52.81	13	3	SR/MM
S23_J	86	S	-72.93	-52.81	22	3	SDF
S42_J	173	S	-72.94	-52.81	53	3	G
S27_J	51	S	-72.92	-52.8	12	3	SDF
S41_J	110	S	-72.36	-52.58	4	3	SR/MM
S40_J	8	S	-72.36	-52.58	14	3	NPR/VR
AGUICER	74	S	-72.12	-45.02	270	4	SDF
ALEBOG	15	S	-72.9	-41.4	100	4	NPR/VR
ALEMIT	70	S	-71.42	-42.58	1000	4	SDF
ALENOR	54	S	-71.63	-42.58	800	4	SDF
ANGOST	111	S	-71.5	-40.83	800	4	NPR/SR
ANTILL	82	S	-72.28	-40.75	730	4	SDF
AUSESQ	112	S	-71.45	-42.83	1100	4	NPR/SR
BAYAS		S	-70.65	-41.37	1100	4	G
CANAMOS	62	S	-71.48	-41.55	700	4	SDF
CARILAF	79	S	-71.63	-39.83	875	4	SDF
CASOVE	151	S	-71.8	-41.18	870	4	G
CERDIE15	57	S	-71.65	-41.3	1500	4	SDF
CERDIE17	81	S	-71.65	-41.3	1750	4	SDF
CERDIE18	56	S	-71.65	-41.3	1800	4	SDF
CEZARE	95	S	-71.67	-41.3	1150	4	SDF
CHALL	152	S	-71.32	-41.25	1250	4	G
CHEQUE		S	-70.67	-41.57	1400	4	G
CHILBORD	48	S	-71.75	-40.67	1000	4	SDF
COLOP	64	S	-71.57	-41.1	1500	4	SDF
COMALLO		S	-70.2	-41.07	815	4	G
CONDOR		S	-71.15	-41.12	800	4	SR/MM
CONFLUEN		S	-71.12	-40.73	690	4	SR/MM
DDTRELA	98	S	-71.7	-40.65	850	4	SDF
ELTEPU		S	-73.13	-41.43	100	4	SR/MM
EPUYZ	163	S	-71.35	-42.31	800	4	G



ESPERA	159	S	-71.85	-42.22	550	4	G
ESQAER	172	S	-71.15	-42.92	780	4	G
ESTGRA		S	-70.67	-41.15	980	4	G
FARWES	156	S	-71.2	-41.22	800	4	G
FUTALE1		S	-71.53	-43.2	380	4	G
FUTALE2	75	S	-71.85	-43.17	330	4	SDF
FUTBOR	113	S	-71.75	-43.17	490	4	NPR/SR
GUALALA	77	S	-72.08	-39.65	450	4	SDF
INGJAC1		S	-69	-41.28	870	4	G
INGJAC2		S	-69.85	-41.33	960	4	G
LANQUIH	143	S	-72.8	-40.97	150	4	NPR/SR
LANQUIV	76	S	-72.53	-41.2	66	4	SDF
LAOLAO	44	S	-71.55	-41.05	765	4	SDF
LAUFCH		S	-69.42	-41.22	800	4	G
LAZETA	164	S	-71.35	-43.9	760	4	G
LGNVER	68	S	-71.57	-39.83	400	4	SDF
LGOCAM	45	S	-71.85	-40.72	1000	4	SDF
LGOCAS	32	S	-71.78	-45.58	1000	4	NPR/VR
LGOCC	17	S	-73.57	-46.18	820	4	NPR/VR
LGOCOR1	65	S	-71.7	-40.6	810	4	SDF
LGOCOR2	73	S	-71.33	-42.87	750	4	SDF
LGOESP	182	S	-72.32	-40.73	525	4	VR
LGOFON	66	S	-71.75	-41.35	750	4	SDF
LGOGAL	83	S	-70	-40.67	950	4	SDF
LGOGUI		S	-71.48	-41.42	950	4	SR/MM
LGOHES	88	S	-71.73	-41.38	740	4	SDF
LGOLAR	63	S	-71.67	-42.67	750	4	SDF
LGOMAL	87	S	-72.33	-43.38	1000	4	SDF
LGOMIR	38	S	-73.43	-46.13	115	4	SDF
LGOMOR	144	S	-71.52	-41.5	800	4	NPR/SR
LGOMOS	71	S	-71.43	-42.5	600	4	SDF
LGONELT	92	S	-71.97	-39.8	200	4	SDF
LGOPAS	165	S	-73.83	-42.37	150	4	VR
LGOPAT		S	-70	-40.67	950	4	Ind
LGOPID		S	-73.07	-41.27	170	4	G
IGOPOP	169	S	-73.47	-42.22	115	4	VR
LGORIE		S	-72.97	-45.5	250	4	G
LGOSAR	78	S	-72.56	-41.5	400	4	SDF
LGOSCH	58	S	-71.5	-41.16	2100	4	SDF
LGOTAR1	167	S	-73.77	-42.72	100	4	VR
LGOTAR2	168	S	-73.77	-42.72	100	4	VR
LGOTOR1	180	S	-72.27	-40.77	700	4	VR
LGOTOR2	181	S	-72.27	-40.77	700	4	VR
LGOTRO	59	S	-71.5	-41.16	2000	4	SDF
LGOVEN1	46	S	-71.67	-41.22	825	4	SDF
LGOVEN2	49	S	-73.02	-45.53	650	4	SDF

LGOVEN3	47	S	-71.67	-41.22	825	4	SDF
LGOYEL	26	S	-72.3	-43.25	546	4	NPR/VR
LLAOL	9	S	-71.55	-41.05	850	4	NPR/VR
LOSCLAR	89	S	-71.82	-41.03	1100	4	SDF
LOSMENU		S	-68.33	-41.08	840	4	G
MALBOO	157	S	-71.58	-41.33	800	4	G
MALLIN	183	S	-72.28	-40.75	750	4	VR
MALLINAU	99	S	-71.68	-41.27	900	4	SDF
MALSON	93	S	-71.53	-41.08	800	4	SDF
MAQUIN		S	-68.63	-41.23	870	4	G
MASCAR	52	S	-71.67	-41.27	800	4	SDF
MATAMOL	161	S	-71	-40.17	1100	4	G
MAUSTR	27	S	-72.47	-43.33	600	4	NPR/VR
MELLIZ		S	-70	-40.67	950	4	Ind
MIRABJ	160	S	-73.45	-40.17	750	4	G
MIRADOR	150	S	-73.45	-40.17	850	4	G
MONTHU	80	S	-71.63	-40.15	640	4	SDF
MYELCH	96	S	-72.47	-43.37	1000	4	SDF
NAHHUA	162	S	-71.17	-41.05	810	4	G
NAHMAP	174	S	-71.17	-39.5	1500	4	G
NAHUH	158	S	-71.34	-41.03	830	4	G
NANTY	114	S	-71.58	-43.17	530	4	NPR/SR
NOTESQ	67	S	-71.47	-42.78	1180	4	SDF
PAMTOR	55	S	-71.45	-41.5	1000	4	SDF
PANQHUE	90	S	-71.78	-40	1100	4	SDF
PASTAHU	170	S	-73.83	-42.37	150	4	VR
PEDREG	154	S	-71.97	-45.57	550	4	G
PILCAN		S	-70.92	-41.11	1000	4	G
PRIMAV	155	S	-71.25	-40.68	800	4	G
PRTMON		S	-72.93	-41.47	100	4	G
PSOTROM	97	S	-71.48	-39.48	11.96	4	SDF
PTOBLES	53	S	-71.8	-41.03	760	4	SDF
PTOCAFE		S	-71.92	-42.72	550	4	SR/MM
PTORAM		S	-72.13	-43.45	300	4	G
QUILLEH	60	S	-71.52	-39.55	1104	4	SDF
REPOL		S	-71.48	-41.88	500	4	SR/MM
RINCON	175	S	-71.07	-41.08	580	4	G
RIOALER	94	S	-71.78	-41.18	850	4	SDF
RIOFRI	179	S	-71.82	-41.02	850	4	VR
RIONEG		S	-73.82	-42.08	60	4	SR/MM
RIOTEP		S	-72.6	-41.25	70	4	G
RUCANAN	69	S	-72.3	-39.55	290	4	SDF
SANANTO	166	S	-73.73	-42.97	150	4	VR
TARAHUB		S	-73.77	-42.72	100	4	G
TRALCAP		S	-72.17	-39.58	230	4	G

786 **Table S2.** List of the 78 pollen taxa.

<b>Family</b>	<b>Taxa name</b>
Rosaceae	<i>Acaena</i>
Fabaceae	<i>Adesmia</i>
Aextoxicaceae	<i>Aextoxicon</i>
Apiaceae	Apiaceae
Araucariaceae	<i>Araucaria</i>
Elaeocarpaceae	<i>Aristotelia</i>
Asteraceae	<i>Artemisia</i>
Asteliaceae	<i>Astelia</i>
Asteraceae	Asteraceae <i>Asteroideae</i>
Asteraceae	Asteraceae <i>Cichorioideae</i>
Flacourtiaceae	<i>Azara</i>
Berberidaceae	<i>Berberis</i>
Boraginaceae	Boraginaceae
Brassicaceae	Brassicaceae
Buddlejaceae	<i>Buddleja</i>
Scrophulariaceae	<i>Calceolaria</i>
Cunoniaceae	<i>Caldcluvia/Eucryphia</i>
Ranunculaceae	<i>Caltha</i>
Caryophyllaceae	Caryophyllaceae
Chenopodiaceae	Chenopodiaceae
Cupressaceae	Cupressaceae
Cyperaceae	Cyperaceae
Podocarpaceae	<i>Dacrydium</i>
Columelliaceae	<i>Desfontainia</i>
Stylidiaceae	<i>Donatia</i>
Winteraceae	<i>Drimys</i>
Proteaceae	<i>Embothrium</i>
Ephedraceae	<i>Ephedra</i>
Ericales	Ericales
Escalloniaceae	<i>Escallonia</i>
Euphorbiaceae	Euphorbiaceae
Fabaceae	Fabaceae
Gentianaceae	Gentianaceae
Geraniaceae	Geraniaceae
Proteaceae	<i>Gevuina/Lomatia</i>
Griselinaceae	<i>Griselinia</i>
Gunneraceae	<i>Gunnera</i>
Hydrangeaceae	<i>Hydrangea</i>
Hydrophylaceae	Hydrophylaceae
Juncaceae	Juncaceae
Santalaceae	<i>Lepidoceras</i>
Philesiaceae	<i>Luzuriaga</i>
Celastraceae	<i>Maytenus</i>

Misodendraceae	<i>Misodendrum</i>
Apiaceae	<i>Mulinum</i>
Myrtaceae	Myrtaceae
Myrtaceae	<i>Myrteola</i>
Nothofagaceae	<i>Nothofagus dombeyi</i> -type
Nothofagaceae	<i>Nothofagus obliqua</i> -type
Onagraceae	Onagraceae
Thymelaeaceae	<i>Ovidia</i>
Hydrophyllaceae	<i>Phacelia</i>
Philesiaceae	<i>Philesia</i>
Plantaginaceae	<i>Plantago</i>
Poaceae	Poaceae
Podocarpaceae	<i>Podocarpus</i>
Polygonaceae	Polygonaceae
Primulaceae	Primulaceae
Araliaceae	<i>Pseudopanax</i>
Ranunculaceae	Ranunculaceae
Rhamnaceae	Rhamnaceae
Verbenaceae	<i>Rhaphithamnus</i>
Grossulariaceae	<i>Ribes</i>
Rosaceae	Rosaceae
Rubiaceae	Rubiaceae
Polygonaceae	<i>Rumex</i>
Salicaceae	<i>Salix</i>
Sapindaceae	Sapindaceae
Podocarpaceae	<i>Saxegothea</i>
Saxifragaceae	Saxifragaceae
Anacardiaceae	<i>Schinus</i>
Scrophulariaceae	Scrophulariaceae
Solanaceae	Solanaceae
Myrtaceae	<i>Tepualia</i>
Urticaceae	<i>Urtica</i>
Valerianaceae	Valerianaceae
Verbenaceae	Verbenaceae
Cunoniaceae	<i>Weinmannia</i>

---

787

788